

Introducing a Concept for Designing an Aqueous Electrolyte with pH Buffer Properties for Zn–MnO₂ Batteries with Mn²⁺/MnO₂ Deposition/Dissolution

Oliver Fitz,* Florian Wagner, Julia Pross-Brakhage, Manuel Bauer, Harald Gentischer, Kai Peter Birke, and Daniel Biro

For large-scale energy-storage systems, the aqueous rechargeable zinc–manganese dioxide battery (ARZMB) attracts increasing attention due to its excellent advantages such as high energy density, high safety, low material cost, and environmental friendliness. Still, the reaction mechanism and its influence on the electrolyte's pH are under debate. Herein, a pH buffer concept for ARZMB electrolytes is introduced. Selection criteria for pH buffer substances are defined. Different buffered electrolytes based on a zinc salt (ZnSO₄, Zn(CH₃COO)₂, Zn(CHOO)₂), and pH buffer substances (acetic acid, propionic acid, formic acid, citric acid, 4-hydrobenzoic acid, potassium bisulfate, potassium dihydrogen citrate, and potassium hydrogen phthalate) are selected and compared to an unbuffered 2 M ZnSO₄ reference electrolyte using titration, galvanostatic cycling with pH tracking, and cyclic voltammetry. By adding buffer substances, the pH changes can be reduced and controlled within the defined operating window, supporting the Mn²⁺/MnO₂ deposition/dissolution mechanism. Furthermore, the potential plateau during discharge can be increased from ≈1.3 V (ZnSO₄) to ≈1.7 V (ZnSO₄ + AA) versus Zn/Zn²⁺ and the energy retention from ≈30% after 268 cycles (ZnSO₄) to ≈86% after 494 cycles (ZnSO₄ + AA). Herein, this work can serve as a basis for the targeted design of long-term stable ARZMB electrolytes.

1. Introduction

The zinc-ion battery (ZIB) with aqueous electrolytes is gaining increasing significance in the scientific literature,^[1–5] as well as for industrial approaches (e.g.,^[6–10]). Within the great variety of active material combinations for the ZIB technology, the acidic aqueous rechargeable zinc–manganese dioxide battery (ARZMB) is a promising technology with great attention in the literature.^[1–5] The reason behind this development is the globally increasing awareness with respect to the critical raw material supply for the prominent lithium-ion battery (LIB) technology.^[11,12] The need for alternative battery cell chemistries is a contemporary topic for the battery research, especially regarding the different fields of application with their respective (and increasing) demands for the battery capabilities.^[13] In this regard, the ARZMB can play an important role for the stationary energy storage (SES), e.g., on- and off-grid, home or peak-shaving storage applications.^[13–17]


Still, the research for ARZMB shows an ongoing and lively debate concerning the reaction mechanism in the aqueous, acidic electrolyte media. Up to now, the reaction mechanisms presented for the ARZMB are mainly as follows: 1) the reversible Zn²⁺ (de-)intercalation;^[18–43] 2) accompanied by the H⁺ (de-)intercalation;^[42–44] and 3) the MnO₂/Mn²⁺ dissolution/deposition.^[29,43–53] a) driven by the proton source available through the Zn/Mn hexa-aqua complexes dissolved in the electrolyte ([Zn(H₂O)₆]²⁺ or [Mn(H₂O)₆]²⁺);^[42,43,53–57] and b) accompanied by the precipitation of zinc hydroxides (ZHs) in the electrode and electrolyte (e.g., zinc hydroxide sulfate [ZHS] in the presence of ZnSO₄).^[42–46,58]

Recent publications in the field of ARZMB emphasize the major contribution of the MnO₂/Mn²⁺ dissolution/deposition mechanism and its influence on the electrolyte's pH value.^[42,46,53–55,59–70] Therefore, pH additives for the electrolytes were introduced to control the electrolyte's pH, listed to the best of our knowledge in **Table 1**.^[46,53–55,62,64–66]

Interestingly, the issues regarding the stabilization of the electrolyte's pH and the uncontrolled dissolution phenomena of the cathode active material are also a field of research within

O. Fitz, F. Wagner, M. Bauer, H. Gentischer, D. Biro
Battery Cell Technology
Department of Electrical Energy Storage
Fraunhofer Institute for Solar Energy Systems ISE
79110 Freiburg, Germany
E-mail: oliver.fitz@ise.fraunhofer.de

J. Pross-Brakhage, K. P. Birke
Electrical Energy Storage Systems
Institute for Photovoltaics (ipv)
University of Stuttgart
70569 Stuttgart, Germany

 The ORCID identification number(s) for the author(s) of this article can be found under <https://doi.org/10.1002/ente.202300723>.

© 2023 The Authors. Energy Technology published by Wiley-VCH GmbH. This is an open access article under the terms of the Creative Commons Attribution-NonCommercial License, which permits use, distribution and reproduction in any medium, provided the original work is properly cited and is not used for commercial purposes.

DOI: 10.1002/ente.202300723

Table 1. Overview over pH additives for ARZMB electrolytes found in the literature so far.

Chemical substance	Chemical formula	Source
Ammonium dihydrogen phosphate Phosphoric acid	$\text{NH}_4^+ \text{H}_2\text{PO}_4^- \text{H}_3\text{PO}_4$	[65]
Ammonium acetate	$\text{NH}_4^+ \text{CH}_3\text{COO}^-$	[53]
Zinc acetate	$\text{Zn}^{2+} (\text{CH}_3\text{COO}^-)_2$	
Ammonia	NH_3	
Acetic acid	CH_3COOH	[46,54,55,62]
Sulfuric acid	H_2SO_4	[66]
Tartaric acid	$\text{C}_4\text{H}_6\text{O}_6$ or $\text{C}_2\text{H}_2(\text{OH})_2(\text{COOH})_2$	[64]

the LIB. Here, the stability of the cathode is influenced by parasitic reactions such as the formation of corrosive acids (here, hydrofluoric acid (HF)) and the acidity of the electrolyte, which lead to the dissolution of transition metals (e.g., Mn in NCM811 cathodes). This phenomenon can be addressed by electrolyte additives (e.g., siloxanes,^[71]), which can form an insoluble interphase film on the cathode and capture corrosive acids. This analogue can be compared to the herein-investigated aqueous ZIB system, where MnO_2 can also uncontrollably be dissolved in the aqueous electrolyte in an acidic environment.

For ARZMB, the main results regarding the electrolyte's pH and the addition of (pH buffer) substances are summarized in the following in chronological order of their year of publication:

Mateos et al.^[54,55] introduced a feasible explanation approach for the functioning mechanism of the ARZMB based on a pH-dependent Nernst equation, highlighting the major role of the $\text{MnO}_2/\text{Mn}^{2+}$ dissolution/deposition mechanism and the Zn/Mn hexa-aqua complexes as the proton source. They showed the influence on the potential curve behavior of pH buffered electrolyte compositions (ECs) using acetic acid (AA) as the buffer solution in different electrolyte compositions, e.g., 1.5 M acetate acid with 0.25 M ZnCl_2 and 0.1 M MnCl_2 , adjusted to pH 5 (pH adjustment with either 2 M KOH or 1 M HCl), and compared them to an unbuffered electrolyte with 0.25 M ZnCl_2 , 0.1 M MnCl_2 , and 0.85 M KCl. The potential curve showed a single stable potential plateau at ≈ 1.55 V versus Zn/Zn^{2+} for buffered electrolytes compared to a steeper potential drop and different potential plateaus at ≈ 1.4 and 1.2 V versus Zn/Zn^{2+} , respectively, for unbuffered electrolytes during discharging, predicted by the pH-dependent Nernst equation.^[54,55]

Guo et al.^[46] used AA to wash cycled MnO_2 cathodes and remove precipitated ZHS from the electrodes after disassembling the cell, reassembled them in new cells and successfully recycled them in 2 M ZnSO_4 electrolyte with recovered discharge capacity. As this treatment of the cathodes does not represent a pH buffering EC, it still shows the importance of controlling the ZHS precipitation and its active material passivation/isolation character by adjusting the electrolyte's pH.^[46]

Li et al.^[66] showed the influence of the electrolyte's pH value on the discharge potential behavior by adjusting either the Mn^{2+} concentration (higher Mn^{2+} concentration reducing the pH) or adding sulfuric acid in the 1 M ZnSO_4 and 1 M MnSO_4 electrolyte.^[66] Higher Mn^{2+} content (here, 3 M) and/or less

pH value by adding sulfuric acid (here, $\text{pH} \approx 2$) stabilized and increased the potential plateau (≈ 1.8 V vs Zn/Zn^{2+}) as well as reduced its steepness. These observation can be related to the results of the publications of Mateos et al. and the formulated pH-dependent Nernst equation mentioned earlier.^[54,55]

Liu et al.^[62] introduced a pH-buffered electrolyte with 1 M ZnSO_4 , 1 M MnSO_4 , and 0.2 M AA ($\text{pH} \approx 2$). This electrolyte showed less pH changes during cycling, a stable potential plateau behavior at > 1.8 V versus Zn/Zn^{2+} during discharging and high Coulombic efficiencies.^[62] These results go in line with the results of the publications mentioned earlier.

Molaei et al.^[64] introduced tartaric acid as pH buffer substance for an ARZMB electrolyte with 2 M ZnSO_4 and 1 M $\text{C}_4\text{H}_6\text{O}_6$. The electrolyte's pH was adjusted to pH 4 by using 0.1 M HCl or NaOH solution. This electrolyte showed a potential plateau at ≈ 1.46 V versus Zn/Zn^{2+} during discharge, good cycling stability, and a capacity in the range of 300–400 mAh g^{-1} .^[64]

Huang et al.^[53] designed and characterized a high-concentrated dual-complex electrolyte based on ammonium acetate ($\text{CH}_3\text{COONH}_4$), zinc acetate (ZA) ($\text{Zn}(\text{CH}_3\text{COO})_2$), ammonia (NH_3), and $\text{Mn}(\text{CH}_3\text{COO})_2$, resulting in an EC with the final molar ratio of 1 M $\text{CH}_3\text{COONH}_4$, 0.4 M NH_3 , 0.2 M $\text{Zn}(\text{CH}_3\text{COO})_2$, 0.075 M $\text{Mn}(\text{CH}_3\text{COO})_2$, and 2 M H_2O , showing an ionic conductivity of 16.1 mS cm^{-1} and an initial pH value of ≈ 7.9 . This electrolyte showed a higher pH stability through its pH buffer capability compared to a reference electrolyte (REL) consisting of ZA and manganese acetate (initial pH value ≈ 5.6). The pH buffer behavior resulted in a potential plateau during discharge at ≈ 1.4 V versus Zn/Zn^{2+} , a good cycling stability, high Coulombic efficiency, and a high areal capacity of 10 mAh cm^{-2} .^[53]

Zhang et al.^[65] used ammonium dihydrogen phosphate (NHP, $\text{NH}_4\text{H}_2\text{PO}_4$) in an EC consisting of 1 M ZnSO_4 and 0.1 M MnSO_4 with 25 mM NHP (initial pH 2.84). This electrolyte showed a stable pH behavior (in Zn||Zn symmetrical cells), a potential plateau at ≈ 1.4 V versus Zn/Zn^{2+} , and a good cycling stability.^[65]

Still, the previously mentioned publications dealing with pH buffer substances are not providing a prior theoretical estimation regarding the stoichiometric ratios of the buffer substances and their interaction, which is influencing the initial pH value and the pH buffer capacity following the Henderson–Hasselbalch equation for pH buffers. Altogether, we could not find a common solution approach in the literature to design the ARZMB electrolytes with pH buffer addition, meeting all the demands for the ARZMB, such as, e.g., the initial pH of the electrolyte and its pH range during operation, the ion concentration for the major electrolyte components such as Zn/Mn salts and the pH buffer substance, as well as their ratio, their electrochemical stability window, and the ionic conductivity of the electrolyte.

Therefore, this work aims at defining the demands for an ARZMB electrolyte with pH buffer properties, based on our previously published studies.^[42,70] Based on these demands, selection criteria for finding appropriate pH buffer substances are formulated and respective substances are selected. Furthermore, the pH buffer capacity of these substances is analyzed by the titration technique with acid and basic titrants. Additionally, theoretical calculations by applying the Henderson–Hasselbalch equation are performed, under consideration and discussion of the underlying assumptions for this equation. Subsequently, an RE consisting of 2 M ZnSO_4 is tested

in cyclic voltammetry (CV) and (long-term) cycling experiments and compared to different EC with pH buffer additives. Finally, recommendations for designing an ARZMB electrolyte with pH buffer capabilities are summarized.

This work can be seen as an important contribution on the way to the solution of the ARZMB electrolyte pH issue to enable long-term stable ARZMB systems for stationary storage applications.

2. Results and Discussion

Reviewing the literature for ARZMB, the standard electrolyte can be defined as an aqueous 2 M ZnSO₄ solution as the electrolyte basis.^[2,42,43] Therefore, this EC will be set as the reference system for the following experiments to, first, clarify the pH challenge within ARZMB electrolytes by showing the acidic and alkaline pH behavior of this aqueous electrolyte solution containing metal ions, and, second, compare modified EC regarding their pH and cycling behavior.

2.1. Reference System

To demonstrate the pH behavior of the (unbuffered) RE 2 M ZnSO₄, this RE was examined in response to a pH change (see Figure 1). The increasing OH⁻ concentration in the cell during cycling was imitated by adding NaOH solution (0.1/1/10 M NaOH, see Experimental Section) and the formation of H⁺ by adding 0.1 M HCl in a titration experiment. This experiment confirms the results of a previous publication by Lee et al.,^[45] which is one of the first publications in the field of ARZMB to highlight the importance of the pH value during operation of the cell.^[45]

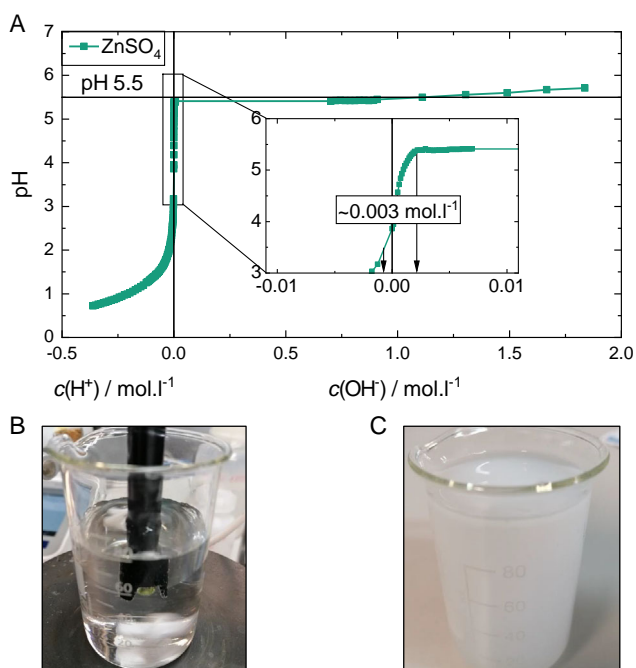
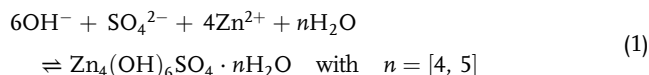


Figure 1. A) Titration curve of the RE 2 M ZnSO₄ titrating it with 0.1 M NaOH and 0.1 M HCl, respectively, as well as the optical comparison of B) the initial look of the solution before and C) the look after the addition of NaOH.

To obtain a general understanding of the buffering mechanisms of the electrolyte, the pH curve in Figure 1 can initially be interpreted qualitatively (a quantitative interpretation will follow in Section 2.2.2): titrating small amounts of OH⁻ ions (NaOH solution), the pH significantly increases. Rapidly, the initially transparent solution turns milky and opaque, indicating the precipitation of a ZH species (here, ZHS, see reaction Equation (1)).^[42,45]



This electrically isolating species buffers the change in pH in the electrolyte, but can lead to the clogging of the porous cathodes and to Zn²⁺ loss within the electrolyte, increasing the inner resistance of the cell, and finally lead to the degradation of the ARZMB cell.^[44,72] Therefore, the control of the pH value in the ARZMB electrolyte is a major task for the long-term stability of the ARZMB and will be addressed in the further scope of this work.

2.2. Identification of Buffer Substances

2.2.1. Selection Criteria

Due to the large choice of potential buffer substances, a definition of selection criteria is required. Finally, the pH buffer substances in question can be selected within the scope of this work based on the defined selection criteria using a funnel approach. Based on patent and literature research on buffer materials, some zinc salts and additives were first collected, which are shown in Figure S2, Supporting Information. Substances or systems that are suitable as pH buffers can usually be described as weak Brønsted acids and their corresponding bases. Due to the—comparatively weak—acid/base character (shown in higher pK_a values in the range of, e.g., $pK_a > 0$ or rather > 3), the substances can be protonated or deprotonated, depending on the pH value, and thus compensate for a pH change in the aqueous medium. As can be seen from the Henderson–Hasselbalch equation (see Equation (S9), Supporting Information), the initial pH value of the EC and the pH buffering behavior can be adjusted by the ratio of the weak acid and a weak base. Due to the specific cell chemistry, there are several requirements for the electrolyte of the ARZMB.

Therefore, the following selection criteria were taken into account for a meaningful selection of materials for the following experiments.

Solubility in Water: A zinc salt should be present as the standard component of the electrolyte. The addition of a manganese salt is often shown in the literature to improve performance, but it is deliberately avoided for this work. The renunciation is based on the guarantee of an electrolyte system that is as binary as possible consisting of preferably two substances to come as close as possible to the mathematical descriptions of buffer solutions according to the Henderson–Hasselbalch equation (see Section 3.4 for further details). In addition, a sufficient ionic conductivity ($> 10 \text{ mS cm}^{-1}$) of the electrolyte is required to reduce Ohmic losses due to resistance in the electrolyte. Supporting electrolytes (e.g., KCl) to increase the ionic conductivity should be avoided, as this reduces the transport of the active

components through migration and further increases the ionic strength.

Furthermore, the concentration of the Zn^{2+} ions influences the energy density of the cell.^[66] Consequently, the solubility of the zinc salt and—at the same time—the concentration of available Zn^{2+} ions must be sufficiently high. To ensure a buffering effect of the electrolyte, the existence of a weak acid and base is necessary and a sufficient solubility of the buffer substances in water is also necessary. Therefore, the solubility is set at $>0.3 \text{ mol L}^{-1}$ within the scope of this work.

Electrochemical Stability: In principle, the electrochemical voltage series can be used to get a first impression of the electrochemical stability of the respective substance based on the possible chemical reactions in an aqueous solution. For this purpose, the considered potential range must be defined: considering the standard electrode potentials of the relevant chemical reactions of Zn/Zn^{2+} , $\text{MnO}_2/\text{Mn}^{2+}$ and H_2/H^+ with respect to the respective reference point such as the standard hydrogen electrode (SHE) at a pH value of 0 (s. standard conditions in the electrochemical series) or the Zn/Zn^{2+} half-cell reaction at pH 0 and pH 4, respectively, potential shifts in the chemical reactions' result, which are visualized in **Figure 2**.^[49,73]

Since zinc is the potential reference in the electrochemical system investigated here, the electrochemical potential versus SHE is transformed into the potentials versus Zn/Zn^{2+} (s. Figure 2B). To enable a dissolution/deposition reaction of $\text{MnO}_2/\text{Mn}^{2+}$ in the system, it is necessary to ensure a sufficient electrochemical potential for this reaction. In a slightly acidic electrolyte at $\text{pH} \approx 4$, the potential for $\text{MnO}_2/\text{Mn}^{2+}$ dissolution/deposition is $\approx 1.518 \text{ V}$ versus Zn/Zn^{2+} (s. Figure 2C). Therefore, the end-of-charge potential must be at least 1.518 V versus Zn/Zn^{2+} or more. Based on the literature, end-of-charge voltages between 1.7 and 1.9 V versus Zn/Zn^{2+} and end-of-discharge voltages between 0.7 and 1 V versus Zn/Zn^{2+} are given. Within the scope of this work, the battery cells are to be cycled in the potential range of 0.7 to 1.8 V versus Zn/Zn^{2+} . To ensure electrochemical stability even at increased voltage ranges (conceivable, e.g., in the context of regeneration cycles or maintenance tasks), a potential range of 0.5 – 2.1 V versus Zn/Zn^{2+} for the EC should be used as a selection criterion.^[4,67,74–77]

The electrochemical stability of the zinc salt and the other electrolyte constituents in the mentioned potential range versus Zn/Zn^{2+} is relevant for the service life of the battery, so that the

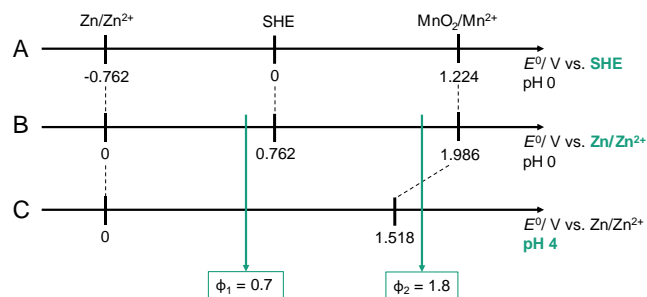


Figure 2. A) Standard potentials of the electrochemical series versus SHE (pH 0) and compared to the visualization versus Zn/Zn^{2+} B) at pH 0 and C) at pH 4.^[55,73,99]

substances are not involved in undesirable side reactions. Therefore, for a selection of the buffer substances in this work, their electrochemical stability in the potential range investigated here was evaluated on the basis of the electrochemical series.^[73]

Dissociation Constant: As many reactions in the ARZMB influence the pH value of the electrolyte, certain pH thresholds must be observed for cycling: 1) The potential pH diagram for zinc (s. Figure S8, Supporting Information) indicates the beginning of a precipitation reaction of a ZH species by means of a vertical line at a pH value of ≈ 5.5 or more^[49,70]; 2) The adapted potential pH diagram for zinc, taking into account the overvoltages for the hydrogen evolution reaction (HER), shows increased corrosion of zinc with the formation of hydrogen from a pH below ≈ 3 ^[78]; 3) The potential-pH diagram for manganese (s. Figure S9, Supporting Information) shows the potential overlapping of the $\text{MnO}_2/\text{Mn}^{2+}$ dissolution/deposition and the oxygen evolution reaction (OER) due to the proximity of the two equilibrium lines to each other. The lower the pH value, the higher the necessary potential for triggering the OER and the potential gap between the OER and the MnO_2 deposition^[49,70]; and 4) As the potential-pH diagram for manganese shows, the electrodeposition of MnO_2 is highly dependent on the potential and pH conditions within the aqueous solution. By this, and especially by the pH conditions, the electrodeposited manganese oxide species can vary, and the disproportionation of Mn^{2+} to Mn^{2+} and Mn^{4+} as well as the formation of MnOOH can take place (latter at higher pH values).^[59,79,80]

The initial pH value of the electrolyte solution should be set within these limits to reduce the OER on the one hand and to avoid the HER with zinc corrosion on the other. Therefore, an initial pH value of $\approx 4 \pm 1$ is sought as a compromise to provide a sufficient pH buffer range.

It should be noted that during the initial material investigations of the selected buffer systems (BSs), the concentration of weak acid is initially kept constant at 0.1 M , which is based on the specifications for standard pH buffer solutions.^[81] By taking into account the dissolved zinc and manganese salts, the BS can be defined based on the Henderson–Hasselbalch equation (s. Equation (S9), Supporting Information).^[73]

Safety and Toxicity: The ARZMB aims at providing an environmentally friendly and harmless storage technology for SES. For this reason, attention should be paid to an environmentally and health-friendly choice of materials during the ARZMB development. Within the framework of these selection criteria, the choice of material is made in compliance with the hazardous substance labeling, whereby highly toxic and oxidizing substances such as sulfides and peroxides or cancerogen mutagen reprotoxic (CMR) substances are to be excluded.

Based on these specifications, different electrolyte systems with three concepts for the formation of an EC with pH buffer properties are formulated within the scope of this work: an additive system (AS), a BS, and a hybrid system (HS) (**Figure 3**).

The AS represents an aqueous system consisting of the standard zinc salt 2 M ZnSO_4 with the addition of a single weak Brønsted acid with the molar concentration of 0.1 M . Therefore, this EC only shows one difference compared to the RE with the aim of buffering the pH and differs mainly in the pK_a values of the added buffer acids.

The BS is also a binary system but consisting of a zinc salt with its conjugate acid. The conceptual design of the BS corresponds

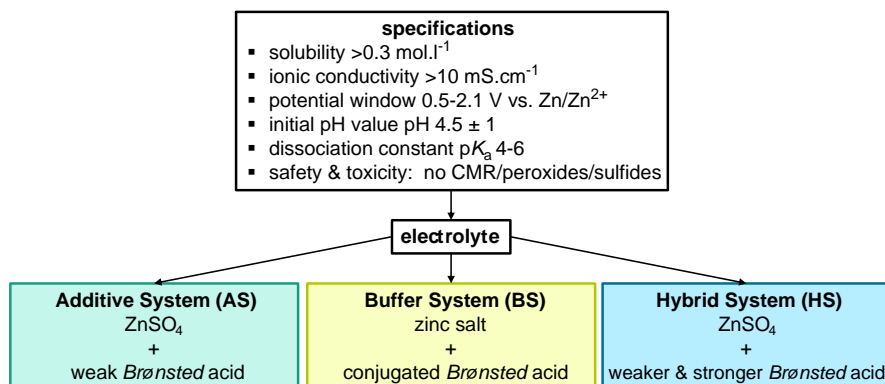


Figure 3. Specifications at the electrolyte of the aqueous rechargeable zinc–manganese dioxide battery (ARZMB) and formulation of the systems for the classification of the different electrolyte composition (EC).

to the characteristic of a pH buffer described in Section S1, Supporting Information. Instead of ZnSO₄, an alternative zinc salt is intended to be used. The advantage of the BS is the possibility of varying the concentration of its buffer base and buffer acid components, which in principle allows the setting of an initial pH value of the electrolyte solution based on the Henderson–Hasselbalch equation. The main challenge in the formulation of the EC of the BS for ARZMB is the sufficient solubility of the zinc salt.

The HS is a ternary system consisting of the established zinc salt ZnSO₄ with the addition of acids with different pK_a values. This allows the targeted adjustment of an initial pH value based

Table 2. Summary of electrolyte specifications for the pH buffer substances within this work.

Parameter	Criterion
Solubility	$>0.3 \text{ mol L}^{-1}$
Ionic conductivity	$>10 \text{ mS cm}^{-1}$
Electrochemical stability in the potential window	0.5–2.1 V versus Zn/Zn ²⁺
Initial pH value	pH 4.5 ± 1
Dissociation constant	$pK_a \approx 4-6$
Safety & toxicity	No CMR substances, peroxides, sulfides

on the dissociation constant of the acids, regardless of the concentration of the added amount.

All substances which meet the selection criteria in Table 2 are further classified. The classification was performed on the basis of the systems presented in Table 3. Detailed properties of the selected acids are listed in Table S1–S5, Supporting Information.

2.2.2. Titration of Buffer Electrolyte Compositions

In the previous chapter, the EC were categorized into three systems. Within this section, the different EC are investigated and compared with the RE 2 M ZnSO₄ in titration experiments to gain insights in the buffer behavior.^[54,55,57]

The results are shown in Figure 4 by plotting the pH value over the standardized hydroxide concentration, which was added as NaOH solution to simulate the pH increase by MnO₂ dissolution when discharging the ARZMB.

First, evaluating the titration curves in Figure 4A, the initial pH value of the different EC significantly differs due to the varying pK_a values of the additives and their constant molar concentrations of 0.1 M, respectively, which influences the buffer capacity. All EC show a pH buffer behavior compared to the RE 2 M ZnSO₄, which can be referred to the significantly delayed pH increase. Also, the EC in Figure 4A shows a similar buffer behavior compared to the titration curves of the different additives without ZnSO₄ addition to the electrolyte (s. Figure S2,

Table 3. Overview of development cooperation divided into the additive system (AS), the buffer system (BS), and the hybrid system (HS).

Additive system (AS)		Buffer system (BS)		Hybrid system (HS)	
2 M zinc sulfate + 0.1 M Brønsted acid		pH 3–4		2 M zinc sulfate + 0, 1 M Brønsted acids in combination	
Inorganic acid	Organic acid	Zinc salt	Conjugated acid	Stronger acid	Weaker acid
Potassium bisulfate (KHS)	4-Hydrobenzoic acid (HBA)	Zinc acetate (ZA, 0.8 M)	Acetic acid (AA, 4.56 M)	Formic acid (FA)	Acetic acid (AA)
Potassium dihydrogen citrate (KDHC)	Propionic acid (PPA)	Zinc formate (ZF, 0.3 M)	Formic acid (FA, 1.69 M)		
Potassium hydrogen phthalate (KHP)	Acetic acid (AA) Citric acid (CA) Formic acid (FA)				

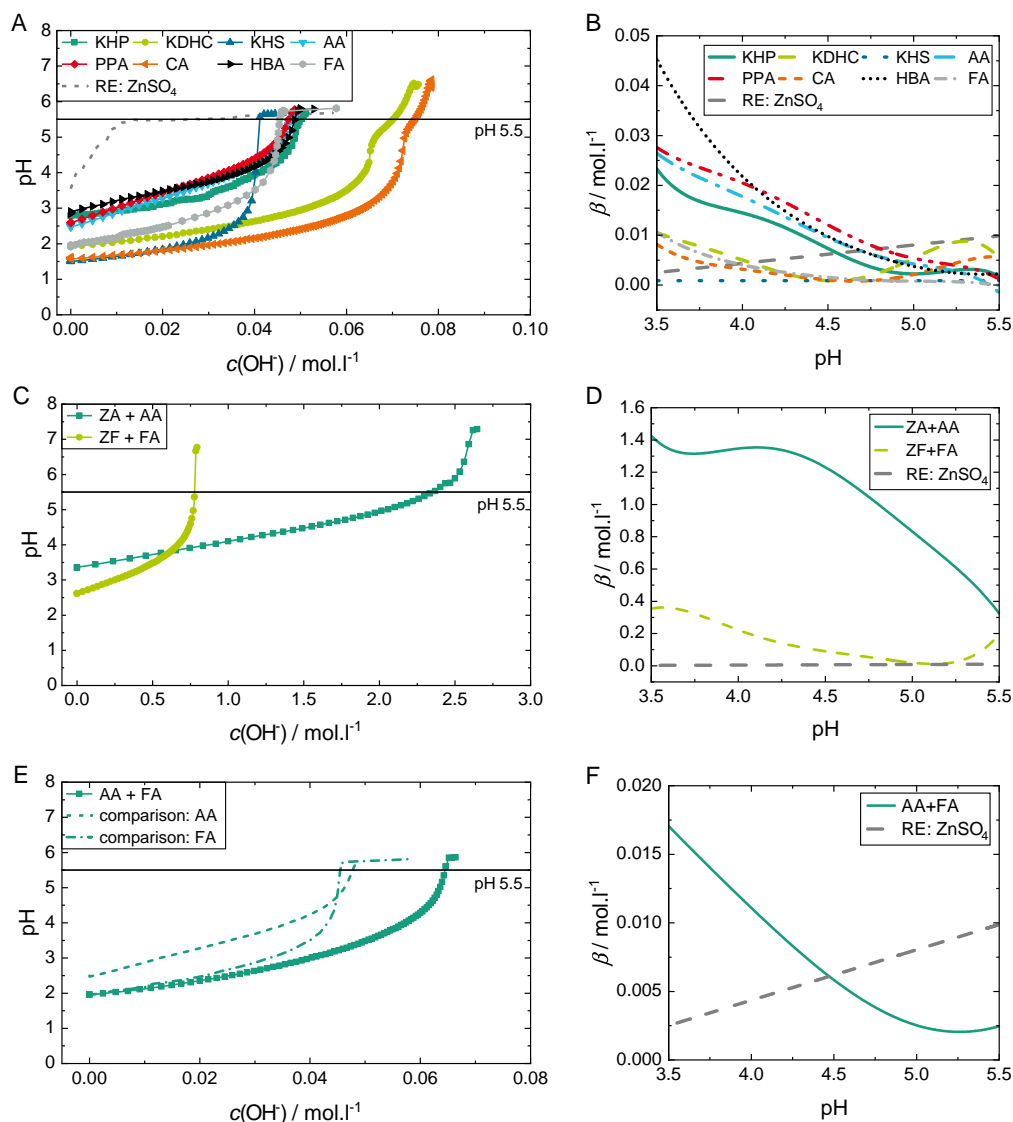


Figure 4. Comparison of the titration curves of A) the additive system (AS), C) the buffer system (BS), and E) the hybrid system (HS), for comparison, the results of FA and AA from the AS are added by the titration with NaOH solution. Furthermore, the pH buffer capacity curves are added for B) the AS, D) BS, and F) HS, respectively, based on the analysis of the titration curves by their fitting and derivation, for a detailed interpretation of the pH buffer behavior within the defined pH working window for each EC.

Supporting Information). Furthermore, it is noticeable that the initial pH value of all EC (in addition to potassium bisulfate [KHS]) is significantly lower when ZnSO_4 is included in the solution. This behavior can be referred to the formation of zinc hexa-aqua complexes $[\text{Zn}(\text{H}_2\text{O})_6]^{2+}$ in an aqueous solution, which have an acidic character ($pK_a = 9$).^[55] Additionally, in addition to potassium dihydrogen citrate (KDHC) and citric acid (CA), the titration curves do not exceed a pH of ≈ 5.5 , where the precipitation of ZHS begins (s. Figure 1). Considering this, since both KDHC and CA contain the citrate group $\text{C}_6\text{H}_5\text{O}_7$, a delayed precipitation of ZHS could be attributed to the complex formation of zinc–citrate complexes in aqueous solution. Nevertheless, in consequence of the multiple dissociation stages in reference to their multiple pK_a values, CA and KDHC have the highest buffer capacities.

The BS provides the possibility to set an initial pH value by using a combination of a base and its conjugate acid using the Henderson–Hasselbalch equation. As for the BS a relatively high acid concentration was added to adjust the initial pH value (s. Table 3), the buffer capacity of the BS is significantly higher than in the AS or HS and the titration results cannot be directly compared to the AS or HS. Furthermore, the BS does not contain any sulfate ions, so that in consequence the precipitation of ZHS cannot take place. Though, another ZH species precipitation can occur which is dependent on the concentration of metal ions in the solution according to reaction (S1, Supporting Information).

In Figure 4C, where the titration curves of the BS with the pH over the added hydroxide concentration are displayed, this can be seen at by a shift of the tipping point to $\approx \text{pH } 7$. The precipitation of ZH during the titration of ZA + acetic acid (ZA + AA) started

at \approx pH 6 in the form of small flakes in the electrolyte (s. Figure 5). Interestingly, ZH exceptionally dissolved again after some time, and only after pH \approx 7 was reached, strong turbidity could be recognized indicating the final tipping point of the ZH precipitation. The delayed precipitation of ZH can also be attributed to the complex formation of zinc–acetate complexes in aqueous solution.

Looking at the titration curve of zinc formate + formic acid (ZF + FA) (Figure 4E), a comparable behavior compared to ZA + AA (s. Figure 4A) can be noticed, but with a reduced pH buffer behavior and a slightly lower initial pH value, which can be referred to the lower overall molar concentration of ZF and FA, as well as to the lower pK_a value of FA.

Within the HS, by the combination of different buffer acids, it is possible to influence the buffer capacity and the initial pH value within the EC. In Figure 4E, the EC with $ZnSO_4 + AA + FA$ as well as the single components +FA and +AA from the AS (s. Figure 4A) for comparison reasons are visualized. This EC combines two Brønsted acids with different pK_a values (here, AA with pK_a 4.76 and FA with pK_a 3.75) with a molar concentration of 0.1 M each. Comparing the HS to the single components from the AS leads to the following interpretations. 1) Looking at the buffer capacities, the HS containing both AA and FA with a total acid concentration of 0.2 M shows a lower buffer capacity than the sum of the single components AA and FA in 0.1 M each (s. Table S7, Supporting Information). Therefore, even though the buffer capacity is dependent on the acid concentration, it seems not linear proportional; 2) Investigating the titration curves characteristic, the curve of the HS shows a comparable behavior than that of the single components of the AS with $ZnSO_4 + AA$ and +FA, respectively. As for the HS, the combination of two acids with different pK_a values in fact results in a pH behavior with a multistage dissociation behavior for each of the pK_a value. As the pK_a values of FA and AA are close to each other, the dissociation stages should be overlapping, resulting in an extended buffer behavior.

A quantification of the buffer capacities is given in Table S7, Supporting Information. The calculation method is shown in Section S4, Supporting Information, based on Equation (S16), Supporting Information. Here, the linear range (criterion: $R^2 > 0.99$) of the pH buffer range and its OH^- concentration

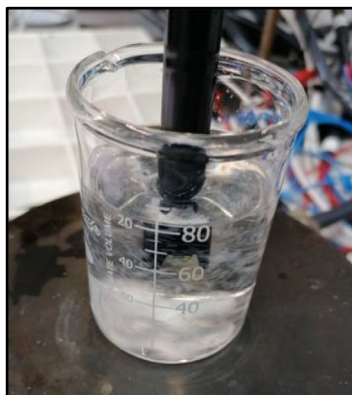


Figure 5. Zinc hydroxide (ZH) precipitation during the titration of 0.1 M NaOH into the EC of the BS.

change is determined. Regarding the results for the pH buffer capacity (either normalized to one pH step, or for the total linear range of the titration curve), within the AS with 0.1 M acid concentration each, the EC $ZnSO_4 + AA$ shows the highest pH buffer capacity. The calculation method can be used for determining the pH buffer capacity regarding the normalized buffer capacity for one pH step, as well as for the linear range of the titration, which follows the literature for the determination of the pH buffer capacity (e.g., ref. [73]).

Still, this calculation method does not give all the necessary information of the pH buffer behavior (e.g., transgression of pH limits such as ZHS precipitation/HER, total pH buffer capacity within pH operation window, etc.) for a specific aqueous system such as the ARZMB. Here, for a quantitative analysis of the buffer capacity behavior within the selected pH operation window of pH 3.5–5.5, the titration curves in Figure 4A,C,D were fitted with a polynomial of 6th grade (s. Figure S4, S5, and S7, Supporting Information, note: x - and y -axis swapped before fitting). Subsequently, the fitting result was differentiated to obtain the behavior of the buffer capacity within the selected pH operation window. The results are shown in Figure 4B,D,F for the AS, BS, and HS, respectively. By this method, the pH buffer behavior in regard of its EC can be analyzed and thereby modified to receive the pH buffer behavior which is needed for the aqueous system (here, ARZMB). The following conclusions can be drawn by interpreting the pH buffer capacity curves. 1) The RE $ZnSO_4$ shows in fact a pH buffer capacity within the selected pH operation window, but on a very slight extent. The pH buffer behavior can mainly be referred to the weak acid strength of the Zn^{2+} ions and their hexa–aqua complex (with a molar concentration of 2 M and low pK_a value of \approx 9, s. provided earlier), enabling a (de-)protonation to a certain degree; 2) The AS generally show low buffer capacities compared to the RE, but only regarding the selected pH operation window of pH 3.5–5.5. In contrast, for the pH buffer range with a linear pH increase of each buffer acid of the AS, the buffer capacity generally significantly exceeds the buffer capacity of the RE (s. Table S7, Supporting Information). This shows the significance of the different pH buffer calculation methods in accordance to the linear range of the titration, or to the defined pH operation window; 3) KDHC (s. Figure 4A) shows high pH buffer capacities within the defined pH operation window for pH values between 3.5 and 4, and again for pH 5.0–5.5, which can be visually analyzed with this introduced evaluation method. This EC property can be used, for example, to specifically shift the maximum pH buffer capacity to these pH regions (e.g., to maximize the pH buffer capacity for the avoidance of the ZHS precipitation at pH \approx 5.5, or to reduce HER at lower pH values \approx 3.5); and 4) The BS of ZA + AA contains 0.8 M ZA and 4.56 M AA, leading to an increased molar concentration and ionic strength of a buffer base and acid in total, and therefore shows an improved pH buffer characteristic. This approach is proved by the significantly higher pH buffer capacity compared to the AS and HS (with lower acid concentrations) and the pH buffer capacity maximum at pH \approx 4.4, which is in the range of the pK_a value for AA of $pK_a = 4.76$. The deviation can be explained by the overall ionic strength of the particular EC of the BS.

The application-oriented approach by defining the pH operation window of the EC for the aqueous system and analyzing the

pH buffer behavior within this operation window (s. Figure 4B, D,F) further helps to design an EC with targeted pH properties.

2.2.3. Cycling of Buffer Electrolyte Compositions

The investigated ECs of the titration experiments are further examined in cycling experiments. The experimental setup is based on our previous study (s. ref. [42]) with the combination of full cell cycling and in-operando pH tracking with a pH sensor (for details, s. Experimental Section). It is noticeable that the initial pH values of the buffered electrolytes (pH 1.5–2.9) are significantly below the initial pH value of the RE 2 M ZnSO₄ (pH 3.35). Regarding the potential-pH diagram of zinc (s. Figure S8, Supporting Information), the Zn corrosion in parallel to the HER is amplified with lower pH values. To prevent this phenomenon and its effect on cycling and pH behavior, an uniform initial pH value of the EC would be necessary. However, this can only be achieved by varying the concentration of the buffer substance or adding an additional substance to adjust the pH, which in turn would change the EC and the molar concentration of the buffer. Due to this trade-off, the uniform buffer acid concentration of 0.1 M is used as a basis for the following cycling experiments for the sake of comparability, and the cycling and pH behavior is evaluated taking into account the influences of a varying initial pH value.

AS: For the AS in Figure 6A1–H1, the potential curves versus Zn/Zn²⁺ and in parallel the pH curves are displayed over time. In addition, in Figure 6A2–H2, the areal discharge capacity per cycle (Q_{DC}) for both the RE and the investigated EC is visualized. The results are compared to the RE ZnSO₄ in Figure 6A + B.

All the pH curves show a pH buffer behavior in terms of the delay of the pH increase within the first few cycles, compared to the RE. Still, differences in terms of the intensity of the pH increase during cycling are observable regarding the buffer substance: For example, KHS (s. Figure 6C1) and FA (s. Figure 6H1) show a stronger pH increase in comparison to the other investigated EC. This is congruent with the titration experiments (s. Figure 4) as KHS and FA show the least system relevant buffer capacities, which can be related to the lower pK_a value of the respective acid and therefore a lower pH buffer capacity in the pH range under consideration. Also, it is conspicuous that the pH curves quickly approach the pH value of ≈ 5.2 when the electrolyte is at rest after the initial 10 cycles. Considering local pH phenomena within the pores of the porous positive carbon fiber electrode by MnO₂ dissolution, during the rest phase, the local phenomena can be measured globally and furthermore, the pH level at pH ≈ 5.2 can be attributed to the pH level of the ZHS precipitation. Observing the pH curves of AA and propionic acid (PPA), but also HBA (note: HBA was not completely soluble in the concentration of 0.1 M), they show the least trend over the 10 cycles compared among all EC.

Regarding the cyclability of the modified EC with buffer acids, it needs to be mentioned that both KDHC and CA could not be cycled properly. After the first few cycles, the capacity already reached zero and no more cycling was possible. Looking at the electrodes after cycling (s. Figure S10, Supporting Information), the cathodes of CA (s. Figure S10A, Supporting Information) and KDHC (s. Figure S10B,

Supporting Information) are fully discharged so that no MnO₂ is visible on the carbon fiber substrate compared to the pristine state after the initial MnO₂ electrodeposition. This is referred to the citrate group which could form stable Mn complexes (high stability constant of complex for [MnHCit]⁻: $\lg K = 3.54\text{--}3.67$)^[82,83] and impede proper Mn²⁺/MnO₂ deposition/dissolution or even the loss of active Mn²⁺.

Regarding the cycle stability compared to the unbuffered RE, the EC of potassium hydrogen phthalate (KHP), KHS, AA, and PPA shows a very similar capacity curve, whereas FA shows significantly lower capacities. For the latter, this behavior can be attributed to the deposition/dissolution behavior of the Mn²⁺/MnO₂ loading of the electrolyte/electrode, which is assumed to be the essential reaction mechanism regarding the latest literature for ARZMB with acid electrolytes.^[29,43–53] The different characteristics of the capacity curves should be examined within long-term stability tests (LSTs), which is performed within Section 3.3.

BS: In Figure 7, the cycling results of the BS electrolytes for A1, A2) ZF + FA and B1, B2) ZA + AA in comparison to A,B) the RE are shown. Here, zinc salts with their conjugated acid were considered.

For the EC-containing ZF + FA (s. Figure 7A1,B1), after the first cycle, the capacity drops to nearly zero and no further cycling can be performed indicating an inactive cell. This behavior can be related to the decomposition of the zinc anode during the first cycle as a result of zinc corrosion/HER (s. Figure S11A, Supporting Information), which was already discussed for the AS with ZnSO₄ + FA.

The EC-containing ZA + AA (s. Figure 7A2,B2), although the capacity is significantly lower compared to the RE, shows a higher capacity stability with even a slight increase in capacity. Furthermore, the pH curve after the 10 cycles stays constant when the cell is at rest. The reduced capacity of the cell can partly be attributed to the reduced ionic conductivity of the EC (s. Table 7) in respect to the RE. An important observation is the formation of salt precipitations around the electrical contacts of the cell cuvette, which only occurs for the EC with higher AA concentration and therefore can be attributed to the AA content of the electrolyte and its evaporation (s. Figure S11B, Supporting Information). This phenomenon could be inhibited by using closed cell formats.

HS: The cycling results for the HS are shown in Figure 8. For these EC, the pH buffering effect and initial pH value can be adjusted by combining two different buffer acids with different pK_a values each. For the combination of AA + FA with ZnSO₄, after a slight initial pH increase, a significant pH buffer behavior is shown with a periodic pH oscillating around pH ≈ 3.25 (s. Figure 8A), which is of higher degree compared to ZnSO₄ + FA. Still, the buffer and cycling behavior both has a comparable characteristic with the EC ZnSO₄ + FA of the AS. This again leads to the conclusion that within the HS, the stronger acid with the lower pK_a value dominates the pH buffer behavior of the EC.

The cycling of the HS confirms the possibility of combining two buffer acids with different chemical properties, whereby targeted buffering effects of the EC can be adjusted. This principle can be transferred to other possible EC and can enable an electrolyte design specifically according to the requirements of the battery cell chemistry.

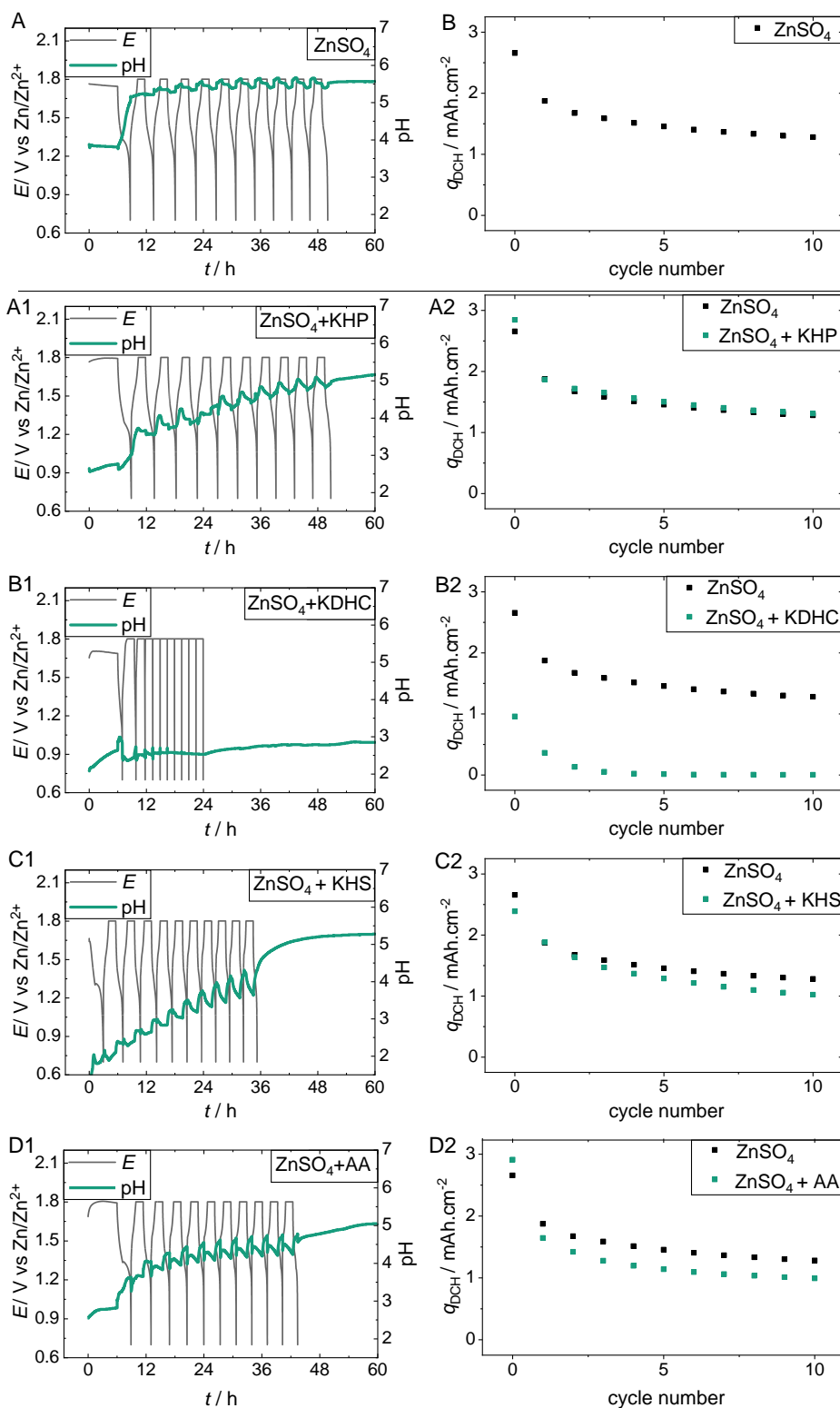


Figure 6. A1–H1) Cycling results of the different EC of the AS showing the potential curve together with the pH behavior, as well as A2–H2) the cycle stability curve for the initial ten cycles, A,B) both compared to the RE 2 M ZnSO₄ without pH buffer capability.

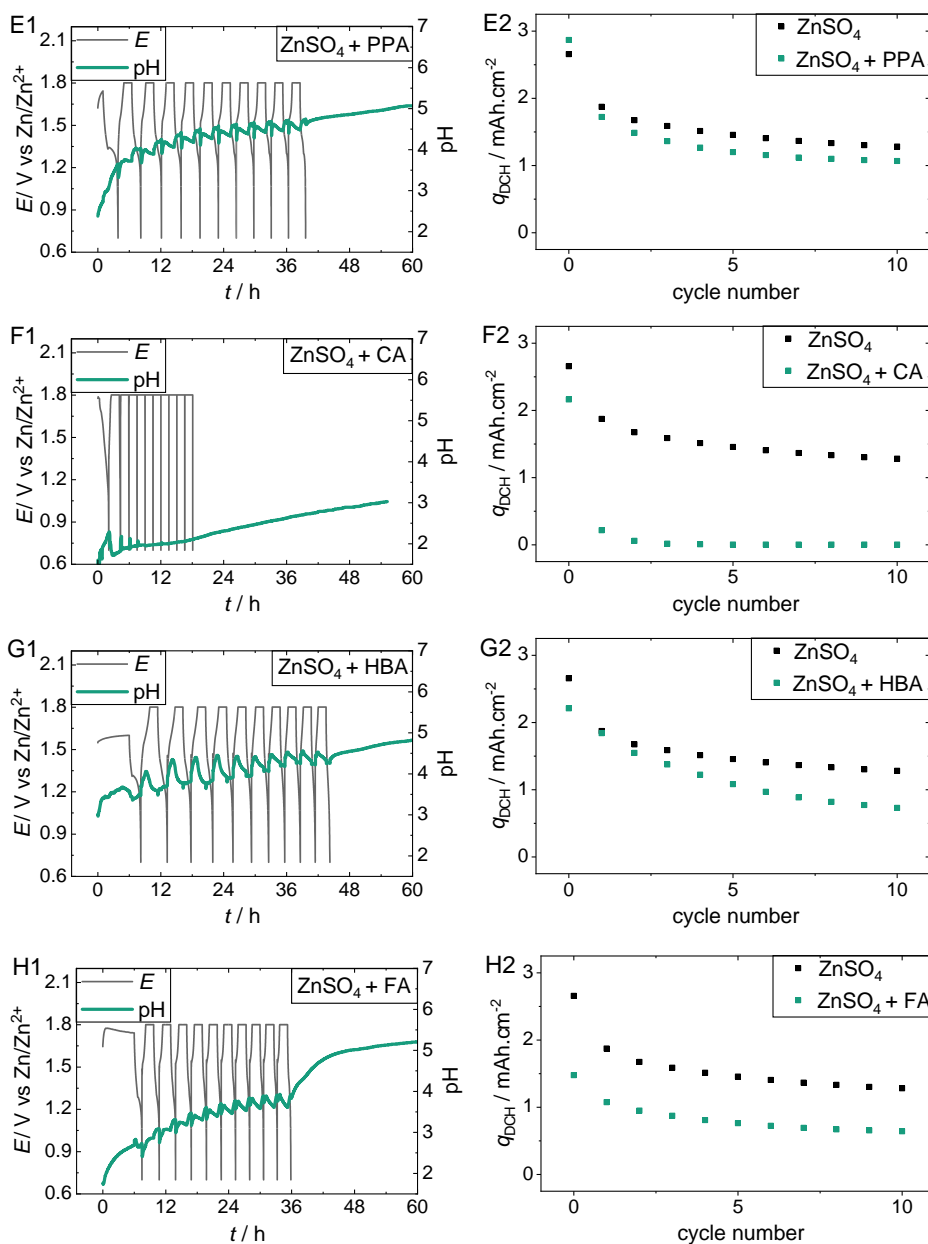


Figure 6. Continued.

In general, after analyzing the experiments, it must be noted that the pH value can only be measured directly in front of the cathode, but not inside the porous electrode. Therefore, the pH results only indirectly represent the local pH behavior at the exact location of the electrochemical reaction (electrode–electrolyte interface). Nevertheless, the reversibility of the pH fluctuations as well as the results of the cells shows that a transferability of the pH fluctuations within the porous electrode is appropriate.

Summary: The potential curves together with the pH behavior of the electrolyte generally show a pH buffering behavior within the first 10 cycles compared to the RE 2 M ZnSO₄. The buffering behavior is indicated by a delayed increase of the pH value in the electrolyte. In principle, the general pH increase of the EC can be

attributed to irreversible gassing reactions (e.g., zinc corrosion with HER). For the AS, in regard to the limited buffer capacity of the buffered EC due to the addition of only 0.1 M buffer acid in the context of this comparative study, the pH buffer can be consumed quickly.

Overall, the discharge capacities for all EC are observed to be either at or below those of the RE ZnSO₄. Among the properly cycled electrolytes, FA in particular shows a significantly lower capacity than ZnSO₄. Various factors must be considered: due to the addition of the buffer substances, the initial pH value in the EC generally drops below the initial pH value of the RE ZnSO₄, which influences zinc corrosion and MnO₂ dissolution as well as the gassing behavior during cycling. Looking at the

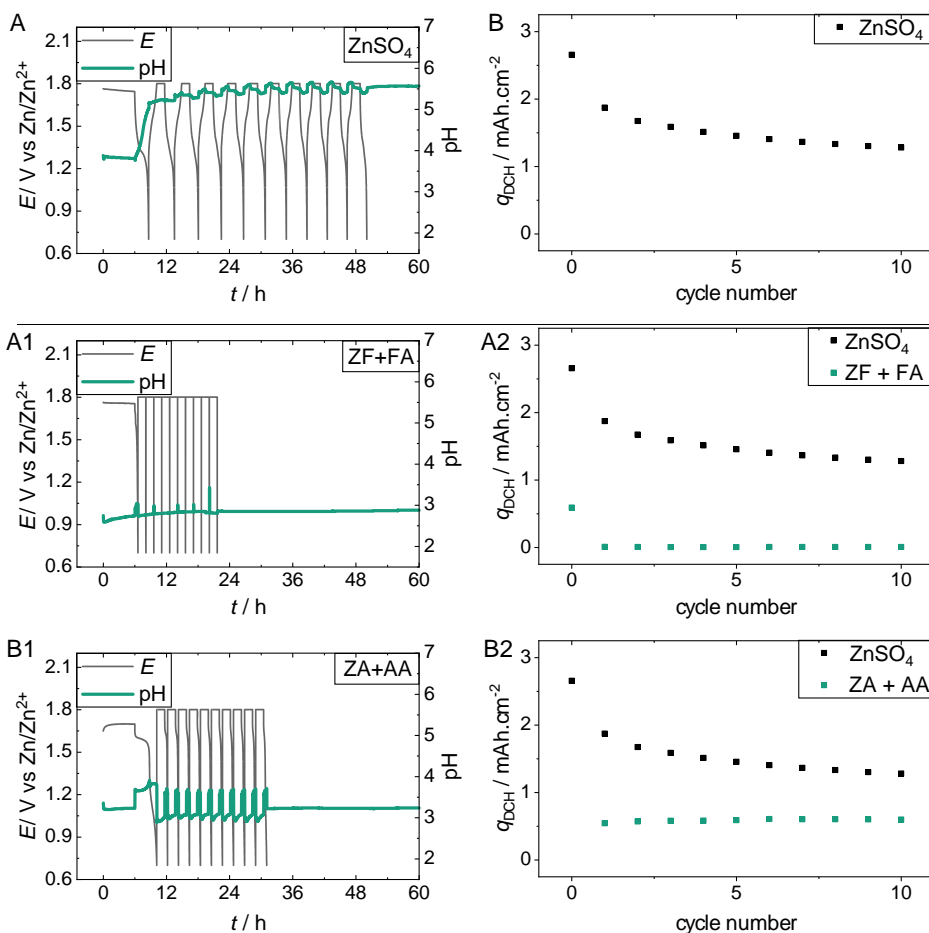


Figure 7. A1, B1) Cycling results of the different EC of the BS showing the potential curve together with the pH behavior, as well as A2, B2) the cycle stability curve for the initial 10 cycles, A, B) both compared to the RE 2 M ZnSO₄ without pH buffer capability.

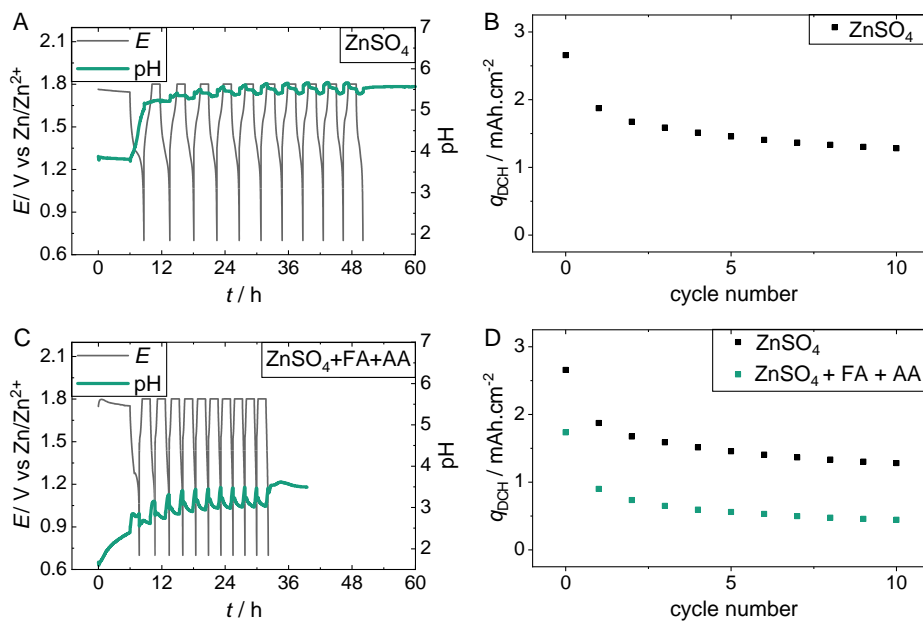


Figure 8. C) Potential and pH curve over time, and D) the areal-specific discharge capacity per cycle for A, B) the cycling experiment within the HS in comparison to the RE.

ionic conductivities (s. Table 7), all EC with 2 M ZnSO₄ are basically in a similar range of $\approx 55 \text{ mS cm}^{-1}$ —with the exception of KHS, which is significantly higher at 62.4 mS cm^{-1} . This may be due to the additional K⁺ ions and/or the additional sulfate anions SO₄²⁻.

2.3. LSTs

To validate the previous results of the buffered EC, the effects on the long-term cycle stability, of stirring as well as of an increased acid concentration, are investigated in comparison to the RE ZnSO₄. Hereto, the pH behavior and the potential plateaus are examined. Based on the results of the previous cycling experiments of the different EC in Section 3.2.3, the best-performing EC were selected for the following LSTs and compared to the RE, in particular ZnSO₄ + AA, ZnSO₄ + PPA, and ZnSO₄ + FA + AA. In advance to the LST, the redox behavior of the selected EC was examined performing CV experiments.

2.3.1. CV for Selected Electrolytes

For a better understanding of the electrochemical behavior of the EC used in the LST, they are further characterized in CV experiments. Thereby, the redox behavior of the different EC is investigated regarding different acid concentration and electrolyte systems.

The results of the CV experiments are displayed in **Figure 9**, whereby on the ordinate, the current is related to the area of active material on the electrode ($A_{\text{electrode}} = 3,75 \text{ cm}^2$).

In **Figure 9A**, the RE shows a typical reduction peak for the first cycle at $\approx 1.25 \text{ V}$ versus Zn/Zn²⁺ and an oxidation peak at $\approx 1.6 \text{ V}$ and 1.8 V versus Zn/Zn²⁺, which refers to the

MnO₂ oxidation and OER, respectively.^[42] For the second cycle, the peak characteristic stays the same, but with slight changes in the peak appearance (e.g., widening of the peaks) which can be referred to changes in the ionic composition of the electrolyte through the Zn²⁺ and Mn²⁺ deposition/dissolution reactions. The other EC based on ZnSO₄ with the addition of acids such as AA (s. **Figure 9B**), PPA (s. **Figure 9C**), and AA + FA (s. **Figure 9D**) show comparable peak characteristics for the first cycle with a distinct reduction and oxidation peak for the Mn²⁺/MnO₂ deposition/dissolution, and a (smaller) second peak, which can be referred to the formation of MnOOH (s. Section 3.2.1). Still, for the second cycle, the peak characteristics significantly change especially for the ZnSO₄ + AA and ZnSO₄ + AA + FA electrolyte. For +AA, the peak characteristic changes to very low current flows. This behavior cannot be deeply explained within this study and needs to be investigated in further studies. A comment on this phenomenon is added to Supporting Information (s. S9). Nevertheless, as the following section shows, this electrolyte still shows a cyclability in full cells. For +AA + FA, the formation of new reduction peaks can be referred to the zinc corrosion behavior, which was already discovered for the pure ZF + FA electrolyte (s. **Figure S11A**, Supporting Information).

Altogether, the CV shows the redox behavior of the electrolytes and a comparable peak characteristic for the different EC compared to the RE ZnSO₄, proving their cyclability. Still, the changes in the peak characteristics for the second cycle need to be related to the cycling behavior within the following section.

2.3.2. Long-Term Cycling

To ensure a homogeneous distribution of the different components of the EC within the electrolyte–electrode interface as well

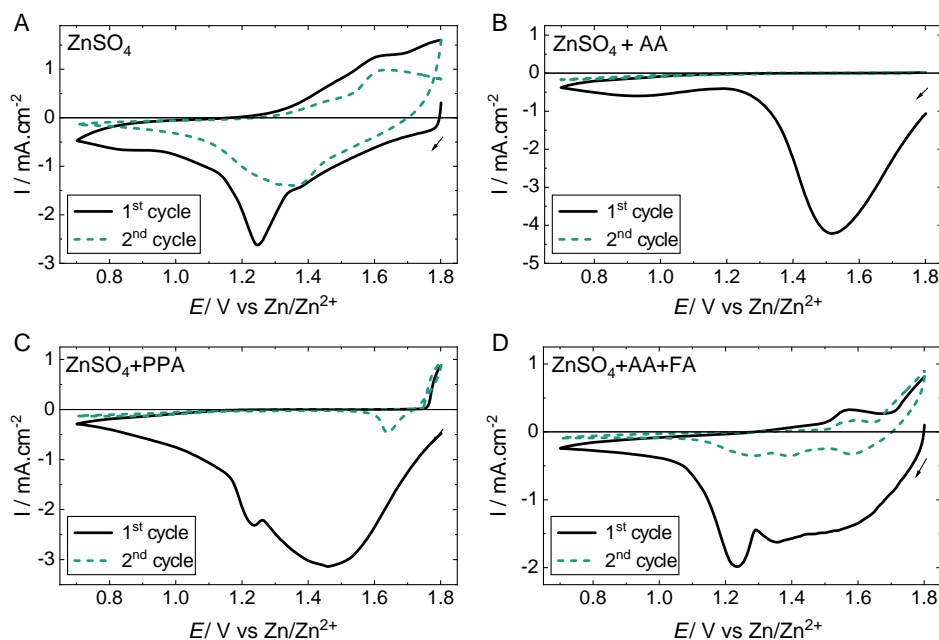


Figure 9. Graphs of the cyclic voltammetry of the EC A) ZnSO₄ (2 M), B) ZnSO₄ + AA (2 M + 1 M), C) ZnSO₄ + PPA (2 M + 0.5 M), and D) ZnSO₄ + AA + FA (2 M + 0.1 M + 0.1 M) for the first two cycles each.

as inside the porous cathode structure, the effect of stirred electrolytes was tested for the LST. This was based on the assumed major reaction mechanism of the $\text{Mn}^{2+}/\text{MnO}_2$ deposition/dissolution, which leads to the importance of a stable pH value in front of and inside the porous cathode structure. Furthermore, the acid concentration within the previous tests, which was set to a fixed value of 0.1 M for a comparative pH buffer study, was modified and increased for AA (from 0.1 to 1 M) and PPA (from 0.1 to 0.5 M) to evaluate the influence of a higher pH buffer concentration on the overall pH buffer capacity and long-term stability.

In **Figure 10**, the stirred electrolytes show a comparable characteristic of periodic pH changes during cycling, as it was observed for the EC in the previous EC buffer cycling tests. Interestingly, looking at the stirred RE ZnSO_4 compared to the cycling experiment without stirring, it becomes visible that the pH oscillations are more pronounced and the pH level for them is slightly lower, even though the critical pH value of ≈ 5.5 is still reached at the end of each discharge cycle. This indicates that due to convection from stirring the electrolyte, the local pH value changes within the porous electrode better become measurable in the bulk electrolyte by stirring or rather mixing the local electrolytic domains. Still, the pH stability for the other EC with AA, PPA, and FA + AA acids addition can be increased and the mass-transport limitation decreased by the stirring, which is shown in a more stable pH level within the first 10 cycles. In addition, for the increased concentration of the acid, a higher pH buffer capacity and therefore a more stable pH level

with smaller periodic pH amplitudes during cycling can be observed.

Generally, observing the pH curve characteristics of the EC with buffer additives in **Figure 10**, after the initial rest phase and initial discharge, the pH curves oscillate around a constant pH plateau without a visible increasing trend. Thereby, regarding $\text{ZnSO}_4 + \text{AA}$ (s. **Figure 10D**), very little oscillations around a very constant pH value are visible which might be a combined effect related to the combination of an increased concentration as well as stirring.

For a closer look at the effect on the EC with buffer acids on the potential curves in **Figure 11A + B**, the first discharge cycle is visualized by plotting the potential versus Zn/Zn^{2+} over the areal discharge capacity q_{DC} . All EC-containing buffer additives show lower discharge capacities compared to the RE. Nevertheless, ECs with increased acid concentrations (1 M AA, 0.5 M PPA) show significantly higher potential plateaus (+AA at ≈ 1.7 V and +PPA at ≈ 1.6 V vs Zn/Zn^{2+}) than the RE (at ≈ 1.2 – 1.4 V vs Zn/Zn^{2+}). Additionally, for the EC $\text{ZnSO}_4 + \text{AA}$, a stable single potential plateau can be observed, which can be explained by the pH-dependent Nernst equation (introduced by Mateos et al. in ref. [55]) and the high pH buffer capacity of the 1 M AA addition. The +AA + FA electrolyte shows two different plateaus comparable to the RE ZnSO_4 , which can be related to the reduction peaks in **Figure 9D**, and which can be explained by zinc corrosion phenomena, as already observed in **Figure S6**, Supporting Information, for FA-containing EC. The effect of the addition of the buffer acids on the potential plateau gets even more

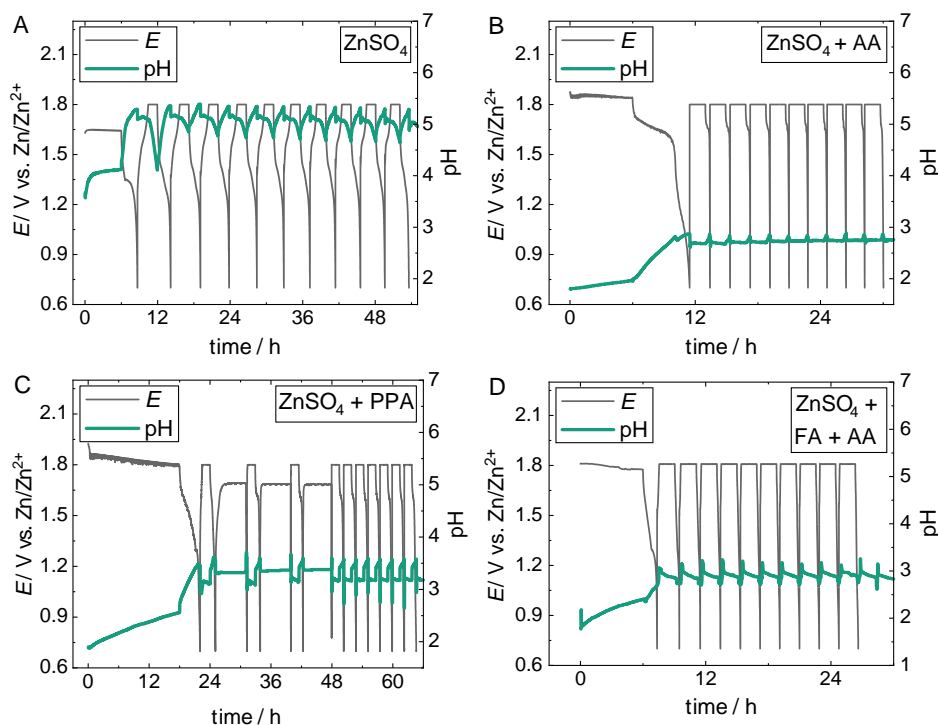


Figure 10. Potential curves in parallel to the pH curves dependent on the time for the first 10 cycles of the long-term stability tests considering stirring for A) the RE ZnSO_4 (2 M), B) $\text{ZnSO}_4 + \text{AA}$ (2 M + 1 M), C) $\text{ZnSO}_4 + \text{PPA}$ (2 M + 0.5 M), and D) $\text{ZnSO}_4 + \text{FA} + \text{AA}$ (2 M + 0.1 M + 0.1 M). Note: C) The open circuit voltage (OCV) phases for the +PPA electrolyte can be ascribed to a test plan bug, but should not affect the cycling behavior, as the pH value also stays constant within the OCV phases.

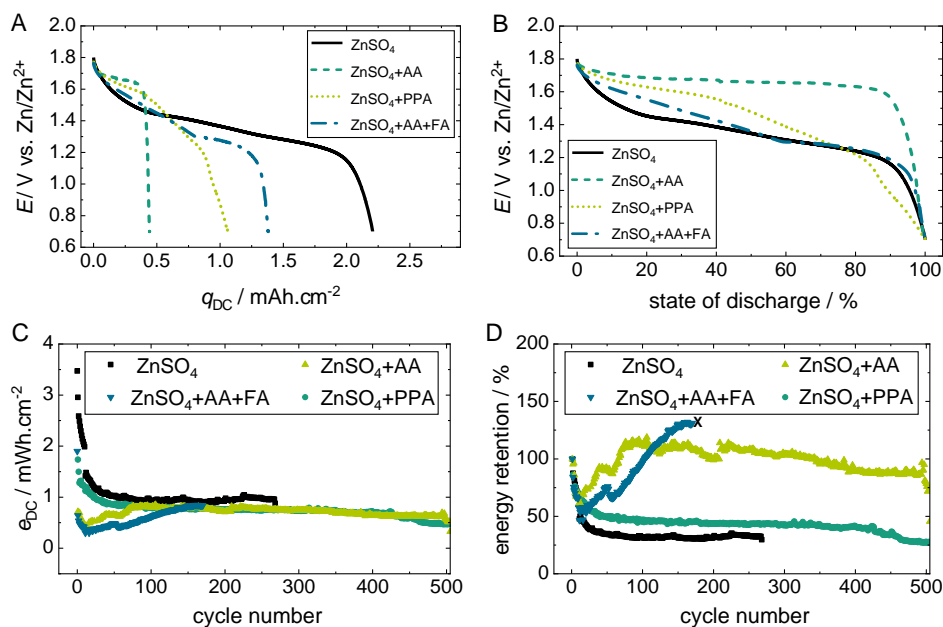


Figure 11. A) Potential curves versus Zn/Zn^{2+} for the selected EC $\text{ZnSO}_4 + \text{AA}$, $+\text{PPA}$, and $+\text{AA} + \text{FA}$ compared to the RE ZnSO_4 over the areal discharge capacity, and B) the same potential curves normalized to the state of discharge. C) The energy curves for the selected EC over the cycle number, and D) the energy retention normalized to the first discharge cycle. Note: The cycling of the $+\text{AA} + \text{FA}$ cell stopped due to zinc corrosion phenomena, in accordance to Figure S6, Supporting Information. The cycling of the RE cell was stopped intentionally.

pronounced by visualizing the potential over the state of discharge (normalized to the first discharge cycle) in Figure 11B.

To consider the effect of higher potential plateaus, for the LSTs in Figure 11C, the areal-specific discharge energy e_{DC} instead of the areal-specific discharge capacity q_{DC} is regarded based on the equation for the energy of a battery ($E = QU$), which better addresses the demands for battery applications. Therefore, in Figure 11C, e_{DC} is shown over the cycle number. Compared to the RE, the energy levels for the EC are generally lower. Still, for the RE in Figure 11C, within the first 30 cycles a strong energy fading can be seen, which is followed by a low energy plateau at $\approx 1.0 \text{ mWh cm}^{-2}$, and which can be attributed to the ZHS precipitation and accumulation (and its pH buffer effect at ≈ 5.5 , s. ref. [42]). In comparison, the initial energy fading of $\text{ZnSO}_4 + \text{AA}$ and $\text{ZnSO}_4 + \text{FA} + \text{AA}$ within the first 30 cycles is lower compared to the first discharge cycle. Furthermore, after the initial energy drop, the energy increases again approaching a constant energy plateau of $\approx 1 \text{ mWh cm}^{-2}$ after ≈ 150 cycles. This behavior gets especially visible in plotting of the energy retention (normalized to the first discharge cycle) over the cycle number (s. Figure 11D). The reason for the strong initial capacity fading with pH buffer additives could be related to the lack of pre-dissolved Mn^{2+} ions, which deteriorates the reversibility of the $\text{Mn}^{2+}/\text{MnO}_2$ deposition/dissolution reaction within the EC, which needs to be investigated in further studies using EC with Mn^{2+} preloading.

Still, as for SES, the energy density is less important than a stable energy and capacity output over many cycles and the lifetime, the lower specific energy level of the EC with buffer additives is acceptable. In contrast, the higher potential plateaus and the stable energy curve is an important finding, which emphasizes the importance of modified EC, especially stabilizing

the pH changes during cycling. In addition, these investigations should serve the further selection of buffer substances and the addition of Mn^{2+} to the EC, which is supported by the herein presented selection criteria for ARZMB applications.

Finally, although stirring showed a positive effect regarding the buffer behavior, the implementation of stirring in a battery stack could be complicated. Therefore, an alternative electrode substrate that is highly porous could help to improve the natural convection in the cell, which is part of further studies.

The most important challenge in the future will be to improve the significantly higher initial energy and capacity fading of electrolyte compositions containing pH buffer additives. Hereto, latest literature reported that the reason for the initial capacity fading might be the lack of Mn^{2+} ions in the electrolyte since no manganese was dissolved in it in advance.^[21,27–29,33,36,46,51,52,60,70,72,84–95] Nevertheless, the significant difference between pure ZnSO_4 and electrolyte compositions containing pH buffer additives regarding the initial energy and capacity loss needs to be further investigated, which will be discussed in the following section.

2.4. Recommendations for Designing Buffer Electrolytes for ARZMB

For the investigations in this study, different EC based on a zinc salt and pH buffering agents are presented. As discussed previously, the preloading of the EC with Mn^{2+} ions leads to a better overall cell performance and cycle stability. Within this study, we deliberately avoided the addition of Mn^{2+} ions to the EC to keep the electrolyte solutions as simple as possible, which is due to the applicability of the Henderson–Hasselbalch equation (s. Equation (S9), Supporting Information). To this equation,

Table 4. Comparison of the assumptions for the validity of the Henderson–Hasselbalch equation and the conditions in the context of the experiments within this study. The green shading indicates a good validity, the yellow shading indicates an approximation, and the red shading indicates no agreement of the conditions for the Henderson–Hasselbalch equation and the experiment.^[100,101]

Conditions Henderson–Hasselbalch equation	Experimental conditions
1. Monobasic acids that release an H ⁺ ion upon dissociation	Valid within the context of the herein considered dissociation degree for all the acids
2. Self-ionization of water negligible (mostly for pH values <10)	Valid in the context of this study
3. Low ion concentrations <1 mol L ⁻¹ , influence of ionic strength neglected	Ion concentrations partly >1 mol L ⁻¹
4. Weak acids with pK _a value between 5 and 9	Mainly valid in the context of this study
5. Binary electrolyte consisting of (weak) acid and corresponding (weak) base	Not valid in the context of the experiments (systems consisting of mixtures of substances)
6. Ultrapure water with pH = 7 ^{a)}	Not given due to open systems, for pH < 5.5, the dissociation is negligible

^{a)}By contact with the atmosphere, CO₂ is absorbed and the pH can drop to ≈5.8.^[100]

the following assumptions apply (s. Table 4). Despite the assumptions for the Henderson–Hasselbalch equation do not fully apply to the herein investigated aqueous system, the equation still helps for demonstrating the concept of designing pH-buffered aqueous electrolytes in acidic environment for ZMB (Table 4).

Based on the equation, the following conclusions can be drawn for the application in the system considered here (Figure 12). According to Equation (S13, Supporting Information), the buffer capacity maximizes at the point pH = pK_a (s. Figure 4D). Furthermore, for the ARZMB with the dissolved Zn²⁺ and Mn²⁺ hexa-aqua complexes, an aqueous system with an acidic character is present. Therefore, buffer acids with pK_a values in the range of the desired pH value of the EC (or slightly above for less acid strength to meet the acidic character of the EC) are necessary to minimize the further reduction of the pH through their addition to the EC. Furthermore, due to their high pK_a value, the acid strength is low, and the dissociation only takes place to a certain degree, leading to a good (de-)protonation behavior for these acids. To map speciation in

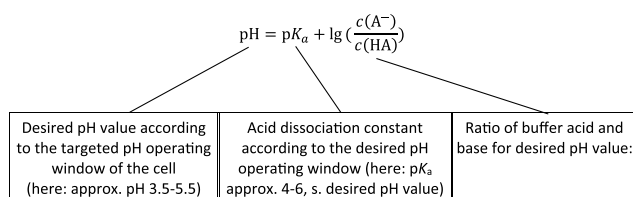


Figure 12. Conclusions for designing pH-buffered electrolytes for ARZMB on the basis of the Henderson–Hasselbalch equation as an aid to understand the pH buffer concept.

Table 5. Summary of the key parameters recommended for EC for ARZMB as a result of this study.

Parameter	Criterion
Molar concentration ratio $c(\text{Zn}^{2+})/c(\text{Mn}^{2+})$	1
Molar concentration $c(\text{Mn}^{2+})$ bzw. $c(\text{Zn}^{2+})$	>0.5 mol L ⁻¹
Initial pH value	pH 4.5 ± 1
pH–operation window	≈3.5–5.5
Ionic conductivity	>10 mS cm ⁻¹
Electrochemical stability in the potential window	0.5–2.1 V versus Zn/Zn ²⁺
Safety & toxicity	No CMR substances, peroxides, sulfides

more complex systems, the resulting nonlinear system of equations must be solved numerically, as implemented for example in common programs such as PHREEQC and MINTEQA2.^[96,97] This type of model could be used in future studies to investigate additional influences such as complexation behavior and the use of multiple electrolyte salts but is beyond the scope of this article.

In addition to the design parameters followed by the Henderson–Hasselbalch equation, the ratio between the Zn²⁺ and Mn²⁺ salt concentration within the EC needs to be set according to the reaction mechanism: as the major reaction mechanism should be based on the Mn²⁺/MnO₂ deposition/dissolution, a Zn²⁺/Mn²⁺ ratio of 1 should consequentially be selected for the EC. By this, the Zn²⁺/Mn²⁺ deposition during charging and the Zn/MnO₂ dissolution during discharging can symmetrically be initiated for the anode and cathode, respectively.

Altogether, the following summary for the key parameters to design a pH–buffer electrolyte for ARZMB in acidic environment can be formulated (Table 5).

3. Conclusion

This study is intended to introduce a general conception for designing pH-buffered electrolytes for the zinc–manganese dioxide battery chemistry with the Mn²⁺/MnO₂ deposition/dissolution. Therefore, in a first step, selection criteria for the buffer substances are defined and different buffer concepts based on a zinc salt as the main component are introduced, such as an AS (ZnSO₄ + acid), a BS (zinc salt + conjugated acid), and an HS (ZnSO₄ + combination of two acids for targeted initial pH value). The contemplable buffer substances are selected based on the selection criteria and the following acids are chosen within this study: AA, PPA, FA, CA, 4-hydrobenzoic acid, KHS, KDHC, and KHP.

For evaluating the buffer behavior of the selected acids, titration experiments are performed for the buffered electrolytes and compared to the RE ZnSO₄. A pH buffer behavior can be proved for all the acids and quantified using titration curves and by introducing the pH buffer capacity behavior by using fitting and derivation techniques of the titration results, respectively.

To validate this finding in full cells, the electrolyte compositions are cycled, and the pH value of the electrolyte is tracked in operando. All the selected electrolytes are cyclable and the

pH buffer behavior can again be proved. Still, for the different acids, impacts on the specific capacity/energy of the cell as well as the capacity/energy curve can be observed.

For testing the impact of the pH-buffered electrolytes on the long-term stability, cycle tests are performed for selected electrolytes with AA, PPA, and the combination of AA and FA. The potential plateau during discharge can be increased from ≈ 1.3 V (ZnSO_4) to ≈ 1.7 V ($\text{ZnSO}_4 + \text{AA}$) versus Zn/Zn^{2+} and the energy retention from $\approx 30\%$ after 268 cycles (ZnSO_4) to $\approx 86\%$ after 494 cycles ($\text{ZnSO}_4 + \text{AA}$).

Altogether, the results can serve as a basis for future electrolyte designing, where the concepts of this study can be used as a fundamental basis to understand, describe and quantify the buffer behavior of ARZMB electrolytes and its impact of the cycle stability for the investigated reaction mechanism. The evaluation of the pH buffer capacity curves within this study can serve as a powerful method for analyzing the pH buffer capacity characteristic of an EC within the defined pH operating window. By this, a targeted electrolyte design for the respective aqueous system, e.g., the ARZMB within this study can be enabled.

4. Experimental Section

Materials: The RE consisted of 2 M ZnSO_4 (Zinc sulfate heptahydrate EMSURE ACS, ISO, Reag. Ph. Eur. For analysis, Supelco, Merck KGaA, Darmstadt, Germany). The electrolytes were prepared depending on their classification and solubilities:

For the electrolytes of the AS, a 2 M ZnSO_4 with 0.1 M of the AS buffer substances was prepared based on the RE. The buffer substances used are listed in **Table 6**.

For the electrolytes of the BS, a solution consisting of 0.8 M ZA (ZA, AnalaR NORMAPUR, VWR Chemicals, Radnor, Pennsylvania, USA) with 4.56 M AA was prepared. In addition, a solution consisting of 0.3 M ZF (ZF 98%, Alfa Aesar, Kandel, Germany) with 1.69 M FA was prepared. Both solutions were adjusted with respect to their mixing ratios of zinc salt with conjugate acid in such a way that an initial pH of 4 was obtained (s. Henderson–Hasselbalch equation).

For the electrolytes of the HS, an electrolyte consisting of 2 M ZnSO_4 with 0.1 M FA and AA each was prepared.

Additionally, for the cycling experiments, to reduce the surface tension of water at the porous cathode, 0.04 M sodium dodecyl sulfate (SDS, USP-NF, BP, Ph. Eur. Pure, pharma grade, ITW Reagents, Darmstadt, Germany) was added to the electrolyte solution which corresponds to the critical micelle concentration of SDS. The EC are summarized in **Table 7**.

Table 6. List of acids for the AS, BS, and HS.

Designation	Chemical formula	Abbreviation	Substance description of the manufacturer
4-hydrobenzoic acid	$\text{C}_7\text{H}_6\text{O}_3$	HBA	4-Hydrobenzoic acid 99%, Alfa Aesar, Kandel, Germany
Acetic acid	$\text{C}_2\text{H}_4\text{O}_2$	AA	Acetic acid puriss. p.a., ACS reagent, reag. ISO, reag. Ph. Eur., $\geq 99.8\%$, Sigma Aldrich, Darmstadt, Germany
Citric acid	$\text{C}_6\text{H}_8\text{O}_7$	CA	Citric acid 99+%, Alfa Aesar, Kandel, Germany
Formic acid	CH_2O_2	FA	Formic acid 98–100% for analysis, Merck KGaA, Darmstadt, Germany
Potassium dihydrogen citrate	$\text{KH}_2\text{C}_6\text{H}_5\text{O}_7$	KDHC	Potassium dihydrogen citrate hydrate ($\approx 15.2\%$ H_2O), 99% (dry basis), Alfa Aesar, Kandel, Germany
Potassium hydrogen phthalate	$\text{KHC}_8\text{H}_4\text{O}_4$	KHP	Technical buffer solution pH 4.01, Mettler Toledo, Gießen, Germany
Potassium hydrogen sulfate	KHSO_4	KHS	Potassium hydrogen sulfate, VWR Chemicals, Radnor, Pennsylvania
Propionic acid	$\text{C}_3\text{H}_6\text{O}_2$	PPA	Propionic acid 99%, Alfa Aesar, Kandel, Germany

Table 7. Summary of the EC within this work.

	Notation	Initial pH	Ionic conductivity [mS cm^{-1}]
Ref.	ZnSO_4	3.55	55.5
AS	2 M $\text{ZnSO}_4 + 0.1$ M PPA	2.59	54.4
	2 M $\text{ZnSO}_4 + 0.1$ M AA	2.47	55.2
	2 M $\text{ZnSO}_4 + 0.1$ M FA	1.92	56.6
	2 M $\text{ZnSO}_4 + 0.1$ M KHS	1.50	62.4
	2 M $\text{ZnSO}_4 + 0.1$ M KHP	2.78	56.0
	2 M $\text{ZnSO}_4 + 0.1$ M KDHC	1.92	55.1
	2 M $\text{ZnSO}_4 + 0.1$ M CA	1.57	56.9
BS	2 M $\text{ZnSO}_4 + 0.1$ M HBA ^{a)}	2.90	54.7
	0.8 M ZA + 4.56 M AA	3.36	10.7
	0.3 M ZF + 1.69 M FA	2.62	22.1
HS	2 M $\text{ZnSO}_4 + 0.1$ M FA + 0.1 M AA	1.95	55.5

^{a)}HBA not completely soluble.

Characterization: The titration tests were carried out using a pH meter (SevenExcellence pH/Cond S470, Mettler Toledo (MT), Gießen, Germany) with the pH electrode MT InLabPro. The titrations took place in a temperature-controlled laboratory at 21 ± 1 °C. In each case, 40 mL of the EC was stirred continuously in a beaker on a magnetic stirrer at 250 rpm. The initial pH of the solution was determined when no pH change could be measured for at least 300 s. Then, the NaOH and HCl solutions (first few titration steps with 0.1 M, then 1 M, and finally 10 M to deplete the buffer capacity) were each added to the solution in reasonable μl increments using a micropipette and the pH and temperature for each step were determined and recorded. The titration data were then combined to map the pH buffer behavior into the basic and acidic ranges. The added volumes of titrant were converted to added concentrations $c(\text{H}^+)$ or $c(\text{OH}^-)$.

In addition, the ionic conductivity was measured at standard conditions for each EC with the conductivity electrode MT InLab710 using the same pH meter MT SevenExcellence pH/Cond S470.

For the comparison of the EC, 10 charge/discharge cycles were initially performed. The following test plan was used for this purpose (s. **Table 8**). The indication of the current rate refers to the amount of MnO_2 pre-deposited by electrodeposition with 37.5 mg per cathode. (**Table 8**)

Cell Assembly: The cell setup for these experiments was designed in such a way that pH measuring during cycling with the electrode MT InLab Semi-Micro was possible (**Figure 13**). Therefore, a cell housing with internal dimensions of $52 \times 29.5 \times 10.5$ mm was fabricated using a 3D

Table 8. Test plan for the cycling experiments with pH measurement for the first 10 cycles of the investigated EC.

#	Designation	Parameter
0	Rest phase	$t = 6$ h
1	Initial discharge (CC)	$i = 100 \text{ mA g}^{-1}$, $E_{\text{DCH}} < 0.7 \text{ V}$ versus Zn/Zn ²⁺
2	Charge (CC)	$i = 100 \text{ mA g}^{-1}$, $E_{\text{CH}} > 1.8 \text{ V}$ versus Zn/Zn ²⁺
3	Charge (CV)	$E_{\text{CH}} = 1.8 \text{ V}$ versus Zn/Zn ²⁺ , $t = 1.5$ h
4	Discharge (CC)	$i = 100 \text{ mA g}^{-1}$, $E_{\text{DCH}} < 0.7 \text{ V}$ versus Zn/Zn ²⁺
5	Loop	#2–4 for 10 cycles

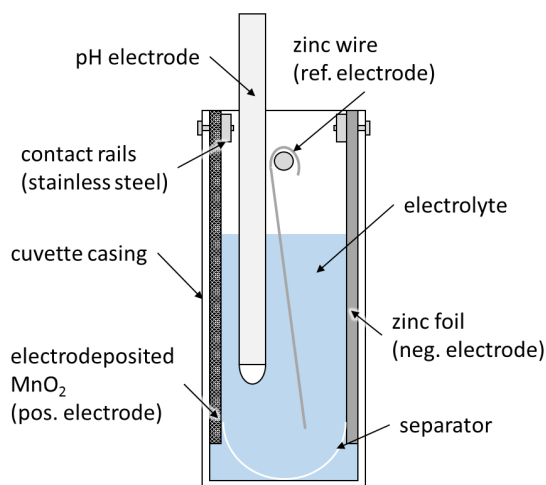


Figure 13. Cell assembly with pH electrode.

printer (Anycubic Photon, Hong Kong Anycubic Technology Co. Ltd., Tsim Sha Tsui, Hong Kong). The contact rails for the electrodes with the dimensions $25 \times 8 \times 2$ mm as well as screws and contact shoes were made of stainless steel (material no. 1.4301) to avoid undesired corrosion reactions. The cathode was prepared by electrodeposition of Mn²⁺ on a carbon fiber substrate with the dimensions of 50×15 mm whereby 30×15 mm were coated with MnO₂ (mass loading 37.5 mg based on a specific mass loading of 10 mg cm^{-2}).^[29,98]

Zinc was used both as anode (zinc foil 99.95%, 25 μm, Goodfellow GmbH, Hamburg, Germany, dimension $50 \times 15 \times 0.025$ mm) and as reference electrode (RE) in the form of a zinc wire (99.9% zinc, Goodfellow GmbH, Hamburg, Germany). To ensure a constant electrode gap (≈ 10 mm) in the cell, a cellulose/polyester separator (Spec-Wipe 3,

Table 9. Test plan for the cyclic voltammetry experiments for the selected EC filtered out for the long-term stability tests.

#	Designation	Parameter
0	Rest phase	$t = 1$ h
1	Lower potential limit	$E_1 \leq 0.7 \text{ V}$ versus Zn/Zn ²⁺
2	Upper potential limit	$E_2 \geq 1.8 \text{ V}$ versus Zn/Zn ²⁺
3	Voltage scan rate	$dE/dt = 0.1 \text{ mV s}^{-1}$
4	No. of cycles	$n = 2$
5	Rest phase	$t = 10$ h

VWR International GmbH, Darmstadt, Germany) was added to the bottom of the cell in a U-shape.

The cycling data was reported with the VMP3 multichannel potentiostat (BioLogic Science Instruments, Seyssinet-Pariset, France). The calibrated pH electrodes were then inserted and aligned in front of the cathode. The electrolyte was added to a level of ≈ 30 mm (electrolyte volume ≈ 9 mL) so that the cathode was completely immersed in it. Finally, the cells were sealed with parafilm.

CV: For the CV experiments, the cell setup mentioned earlier in Cell assembly and Characterization (s. also Figure 13) was used but without pH tracking. The parameters used for the potentiostat are summarized in **Table 9**.

Supporting Information

Supporting Information is available from the Wiley Online Library or from the author.

Acknowledgements

This work was funded by the German Federal Fellowship (Deutsche Bundesstiftung Umwelt, DBU).

Open Access funding enabled and organized by Projekt DEAL.

Conflict of Interest

The authors declare no conflict of interest.

Data Availability Statement

The data that support the findings of this study are available from the corresponding author upon reasonable request.

Keywords

aqueous batteries, electrochemistry, pH buffers, pH buffer capacities, titrations, zinc–manganese dioxide batteries

Received: June 29, 2023

Revised: August 10, 2023

Published online: September 3, 2023

- [1] U. Fegade, G. Jethave, F. Khan, A. Al-Ahmed, R. Karmouch, M. Shariq, Inamuddin, M. F. Ahmer, *Int. J. Energy Res.* **2022**, *46*, 13152.
- [2] Y. Wang, Z. Wang, F. Yang, S. Liu, S. Zhang, J. Mao, Z. Guo, *Small* **2022**, *18*, 2107033.
- [3] J. Song, K. Xu, N. Liu, D. Reed, X. Li, *Mater. Today* **2021**, *45*, 191.
- [4] N. Wang, X. Qiu, J. Xu, J. Huang, Y. Cao, Y. Wang, *ACS Mater. Lett.* **2022**, *4*, 190.
- [5] Z. Tie, Z. Niu, *Angew. Chem. Int. Ed.* **2020**, *59*, 21293.
- [6] E. Bellini, *Salient Energy Develops Zinc-Ion Battery for Residential Applications*, pv Magazine, Berlin, Germany **2022**.
- [7] B. D. Adams, US20200176198A1, **2018**.
- [8] Enerpoly. Sustainable Batteries for Energy Storage, <https://enerpoly.com/> (accessed: May 2022).
- [9] Eos Energy Enterprises, <https://eosenergystorage.com/> (accessed: May 2022).
- [10] Urban Electric Power, <https://urbanelectricpower.com/> (accessed: May 2021).
- [11] P. Ferro, F. Bonollo, *Sustainable Mater. Technol.* **2023**, *35*, e00543.

- [12] S. Windisch-Kern, E. Gerold, T. Nigl, A. Jandric, M. Altendorfer, B. Rutrecht, S. Scherhauer, H. Raupenstrauch, R. Pomberger, H. Antrekowitsch, F. Part, *Waste Manage.* **2022**, *138*, 125.
- [13] Y. Zhao, O. Pohl, A. I. Bhatt, G. E. Collis, P. J. Mahon, T. Rütther, A. F. Hollenkamp, *Sustainable Chem.* **2021**, *2*, 167.
- [14] J. Geng, S. Gao, X. Sun, Z. Liu, F. Zhao, H. Hao, *Energy* **2022**, *253*, 124159.
- [15] Z. Zhu, T. Jiang, M. Ali, Y. Meng, Y. Jin, Y. Cui, W. Chen, *Chem. Rev.* **2022**, *122*, 16610.
- [16] M. Yan, H. Ni, H. Pan, *Adv. Energy Sustainability Res.* **2020**, *1*, 2000026.
- [17] X. Fan, B. Liu, J. Liu, J. Ding, X. Han, Y. Deng, X. Lv, Y. Xie, B. Chen, W. Hu, C. Zhong, *Trans. Tianjin Univ.* **2020**, *26*, 92.
- [18] C. Xu, H. Du, B. Li, F. Kang, Y. Zeng, *Electrochem. Solid-State Lett.* **2009**, *12*, A61.
- [19] C. Xu, S. W. Chiang, J. Ma, F. Kang, *J. Electrochem. Soc.* **2012**, *160*, A93.
- [20] C. Xu, B. Li, H. Du, F. Kang, *Angew. Chem.* **2012**, *51*, 933.
- [21] D. Xu, B. Li, C. Wei, Y.-B. He, H. Du, X. Chu, X. Qin, Q.-H. Yang, F. Kang, *Electrochim. Acta* **2014**, *133*, 254.
- [22] M. H. Alfaruqi, J. Gim, S. Kim, J. Song, D. T. Pham, J. Jo, Z. Xiu, V. Mathew, J. Kim, *Electrochem. Commun.* **2015**, *60*, 121.
- [23] M. H. Alfaruqi, V. Mathew, J. Gim, S. Kim, J. Song, J. P. Baboo, S. H. Choi, J. Kim, *Chem. Mater.* **2015**, *27*, 3609.
- [24] M. H. Alfaruqi, J. Gim, S. Kim, J. Song, J. Jo, S. Kim, V. Mathew, J. Kim, *J. Power Sources* **2015**, *288*, 320.
- [25] M. H. Alfaruqi, S. Islam, J. Gim, J. Song, S. Kim, D. T. Pham, J. Jo, Z. Xiu, V. Mathew, J. Kim, *Chem. Phys. Lett.* **2016**, *650*, 64.
- [26] N. Zhang, F. Cheng, Y. Liu, Q. Zhao, K. Lei, C. Chen, X. Liu, J. Chen, *J. Am. Chem. Soc.* **2016**, *138*, 12894.
- [27] W. Sun, F. Wang, S. Hou, C. Yang, X. Fan, Z. Ma, T. Gao, F. Han, R. Hu, M. Zhu, C. Wang, *J. Am. Chem. Soc.* **2017**, *139*, 9775.
- [28] N. Zhang, F. Cheng, J. Liu, L. Wang, X. Long, X. Liu, F. Li, J. Chen, *Nat. Commun.* **2017**, *8*, 405.
- [29] M. Chamoun, W. R. Brant, C.-W. Tai, G. Karlsson, D. Noréus, *Energy Storage Mater.* **2018**, *15*, 351.
- [30] M. H. Alfaruqi, S. Islam, D. Y. Putro, V. Mathew, S. Kim, J. Jo, S. Kim, Y.-K. Sun, K. Kim, J. Kim, *Electrochim. Acta* **2018**, *276*, 1.
- [31] J. Hao, J. Mou, J. Zhang, L. Dong, W. Liu, C. Xu, F. Kang, *Electrochim. Acta* **2018**, *259*, 170.
- [32] B. Wu, G. Zhang, M. Yan, T. Xiong, P. He, L. He, X. Xu, L. Mai, *Small* **2018**, *14*, 1703850.
- [33] Y. Li, S. Wang, J. R. Salvador, J. Wu, B. Liu, W. Yang, J. Yang, W. Zhang, J. Liu, J. Yang, *Chem. Mater.* **2019**, *31*, 2036.
- [34] X. Wang, S. Zheng, F. Zhou, J. Qin, X. Shi, S. Wang, C. Sun, X. Bao, Z.-S. Wu, *Natl. Sci. Rev.* **2020**, *7*, 64.
- [35] S. Yang, M. Zhang, X. Wu, X. Wu, F. Zeng, Y. Li, S. Duan, D. Fan, Y. Yang, X. Wu, *J. Electroanal. Chem.* **2019**, *832*, 69.
- [36] C. Qiu, X. Zhu, L. Xue, M. Ni, Y. Zhao, B. Liu, H. Xia, *Electrochim. Acta* **2020**, *351*, 136445.
- [37] S. Khamsanga, R. Pornprasertsuk, T. Yonezawa, A. A. Mohamad, S. Kheawhom, *Sci. Rep.* **2019**, *9*, 8441.
- [38] J. S. Ko, M. B. Sassin, J. F. Parker, D. R. Rolison, J. W. Long, *Sustainable Energy Fuels* **2018**, *2*, 626.
- [39] T. Yamamoto, T. Shoji, *Inorg. Chim. Acta* **1986**, *117*, L27.
- [40] J. Lee, J. B. Ju, W. I. Cho, B. W. Cho, S. H. Oh, *Electrochim. Acta* **2013**, *112*, 138.
- [41] B. Lee, C. S. Yoon, H. R. Lee, K. Y. Chung, B. W. Cho, S. H. Oh, *Sci. Rep.* **2014**, *4*, 6066.
- [42] O. Fitz, C. Bischoff, M. Bauer, H. Gentscher, K. P. Birke, H.-M. Henning, D. Biro, *ChemElectroChem* **2021**, *8*, 3553.
- [43] N. Zhang, J.-C. Wang, Y.-F. Guo, P.-F. Wang, Y.-R. Zhu, T.-F. Yi, *Coord. Chem. Rev.* **2023**, *479*, 215009.
- [44] L. Li, T. K. A. Hoang, J. Zhi, M. Han, S. Li, P. Chen, *ACS Appl. Mater. Interfaces* **2020**, *12*, 12834.
- [45] B. Lee, H. R. Seo, H. R. Lee, C. S. Yoon, J. H. Kim, K. Y. Chung, B. W. Cho, S. H. Oh, *ChemSusChem* **2016**, *9*, 2948.
- [46] X. Guo, J. Zhou, C. Bai, X. Li, G. Fang, S. Liang, *Mater. Today Energy* **2020**, *16*, 100396.
- [47] G. Liang, F. Mo, H. Li, Z. Tang, Z. Liu, D. Wang, Q. Yang, L. Ma, C. Zhi, *Adv. Energy Mater.* **2019**, *9*, 1901838.
- [48] P. W. Atkins, J. de Paula, *Physical Chemistry*, W.H. Freeman and Co, New York **2010**.
- [49] M. Pourbaix, *Atlas of Electrochemical Equilibria in Aqueous Solutions*, NACE International, Houston **1974**.
- [50] D. Perez-Antolin, I. Sáez-Bernal, A. Colina, E. Ventosa, *Electrochem. Commun.* **2022**, *138*, 107271.
- [51] X. Shen, X. Wang, Y. Zhou, Y. Shi, L. Zhao, H. Jin, J. Di, Q. Li, *Adv. Funct. Mater.* **2021**, *31*, 2101579.
- [52] H. Chen, S. Cai, Y. Wu, W. Wang, M. Xu, S.-J. Bao, *Mater. Today Energy* **2021**, *20*, 100646.
- [53] J. Huang, X. Chi, J. Wu, J. Liu, Y. Liu, *Chem. Eng. J.* **2022**, *430*, 133058.
- [54] M. Mateos, N. Makivic, Y.-S. Kim, B. Limoges, V. Balland, *Adv. Energy Mater.* **2020**, *10*, 2000332.
- [55] M. Mateos, K. D. Harris, B. Limoges, V. Balland, *ACS Appl. Energy Mater.* **2020**, *3*, 7610.
- [56] V. Balland, M. Mateos, A. Singh, K. D. Harris, C. Laberty-Robert, B. Limoges, *Small* **2021**, *17*, 2101515.
- [57] Y.-S. Kim, K. D. Harris, B. Limoges, V. Balland, *Chem. Sci.* **2019**, *10*, 8752.
- [58] Y. Huang, J. Mou, W. Liu, X. Wang, L. Dong, F. Kang, C. Xu, *Nano Micro Lett.* **2019**, *11*, 860.
- [59] C. Xie, T. Li, C. Deng, Y. Song, H. Zhang, X. Li, *Energy Environ. Sci.* **2020**, *13*, 135.
- [60] X. Zeng, J. Liu, J. Mao, J. Hao, Z. Wang, S. Zhou, C. D. Ling, Z. Guo, *Adv. Energy Mater.* **2020**, *10*, 1904163.
- [61] J. Lei, Y. Yao, Z. Wang, Y.-C. Lu, *Energy Environ. Sci.* **2021**, *14*, 4418.
- [62] Z. Liu, Y. Yang, S. Liang, B. Lu, J. Zhou, *Small Struct.* **2021**, *2*, 2100119.
- [63] Y. Liu, Z. Qin, X. Yang, J. Liu, X.-X. Liu, X. Sun, *ACS Energy Lett.* **2022**, *7*, 1814.
- [64] E. Molaei, M. M. Doroodmand, R. Shaali, *Sci. Rep.* **2022**, *12*, 13301.
- [65] W. Zhang, Y. Dai, R. Chen, Z. Xu, J. Li, W. Zong, H. Li, Z. Li, Z. Zhang, J. Zhu, F. Guo, X. Gao, Z. Du, J. Chen, T. Wang, G. He, I. P. Parkin, *Angew. Chem. Int. Ed.* **2023**, *62*, e202212695.
- [66] G. Li, W. Chen, H. Zhang, Y. Gong, F. Shi, J. Wang, R. Zhang, G. Chen, Y. Jin, T. Wu, Z. Tang, Y. Cui, *Adv. Energy Mater.* **2020**, *10*, 1902085.
- [67] Y.-P. Deng, R. Liang, G. Jiang, Y. Jiang, A. Yu, Z. Chen, *ACS Energy Lett.* **2020**, *5*, 1665.
- [68] R. N. de Guzman, A. Awaluddin, Y.-F. Shen, Z. R. Tian, S. L. Suib, S. Ching, C.-L. O'Young, *Chem. Mater.* **1995**, *7*, 1286.
- [69] P. Ruan, S. Liang, B. Lu, H. J. Fan, J. Zhou, *Angew. Chem. Int. Ed.* **2022**, *61*, e202200598.
- [70] C. F. Bischoff, O. S. Fitz, J. Burns, M. Bauer, H. Gentscher, K. P. Birke, H.-M. Henning, D. Biro, *J. Electrochem. Soc.* **2020**, *167*, 20545.
- [71] Y. Chen, Q. He, Y. Mo, W. Zhou, Y. Zhao, N. Piao, C. Liu, P. Xiao, H. Liu, B. Li, S. Chen, L. Wang, X. He, L. Xing, J. Liu, *Adv. Energy Mater.* **2022**, *12*, 2201631.
- [72] O. Fitz, S. Ingenhoven, C. Bischoff, H. Gentscher, K. P. Birke, D. Saracsan, D. Biro, *Batteries* **2021**, *7*, 40.
- [73] *A Ready-Reference Book of Chemical and Physical Data* (Ed: W. M. Haynes), CRC Press, Boca Raton; London; New York **2017**.
- [74] K. Cai, S.-H. Luo, J. Feng, J. Wang, Y. Zhan, Q. Wang, Y. Zhang, X. Liu, *Chem. Rec.* **2021**, *22*, e202100169.

- [75] X. Luo, W. Peng, Y. Li, F. Zhang, X. Fan, *Green Energy Environ.* **2021**, *7*, 858.
- [76] X. Jia, C. Liu, Z. G. Neale, J. Yang, G. Cao, *Chem. Rev.* **2020**, *120*, 7795.
- [77] T. Xue, H. J. Fan, *J. Energy Chem.* **2021**, *54*, 194.
- [78] T. K. A. Hoang, T. N. L. Doan, K. E. K. Sun, P. Chen, *RSC Adv.* **2015**, *5*, 41677.
- [79] T.-H. Wu, Y.-Q. Lin, Z. D. Althouse, N. Liu, *ACS Appl. Energy Mater.* **2021**, *4*, 12267.
- [80] C. P. Yi, S. R. Majid, in *Semiconductors - Growth and Characterization* (Eds.: R. Inguanta, C. Sunseri), InTech, London, UK **2018**.
- [81] *Pufferlösung PH 4.01. Sicherheitsdatenblatt*, Mettler-Toledo GmbH, Greifensee, Schweiz **2021**.
- [82] D. Wyrzykowski, L. Chmurzyński, *J. Therm. Anal. Calorim.* **2010**, *102*, 61.
- [83] J. J. Morgan, *Geochim. Cosmochim. Acta* **2005**, *69*, 35.
- [84] Z. Zhong, J. Li, L. Li, X. Xi, Z. Luo, G. Fang, S. Liang, X. Wang, *Energy Storage Mater.* **2022**, *46*, 165.
- [85] H. Chen, C. Dai, F. Xiao, Q. Yang, S. Cai, M. Xu, H. J. Fan, S.-J. Bao, *Adv. Mater.* **2022**, *34*, 2109092.
- [86] T. Sun, Q. Nian, S. Zheng, J. Shi, Z. Tao, *Small* **2020**, *16*, 2000597.
- [87] N. Becknell, P. P. Lopes, T. Hatsukade, X. Zhou, Y. Liu, B. Fisher, D. Y. Chung, M. G. Kanatzidis, N. M. Markovic, S. Tepavcevic, V. R. Stamenkovic, *Adv. Funct. Mater.* **2021**, *31*, 2102135.
- [88] M. Fayette, H. J. Chang, I. A. Rodríguez-Pérez, X. Li, D. Reed, *ACS Appl. Mater. Interfaces* **2020**, *12*, 42763.
- [89] Y. Zhong, X. Xu, J.-P. Veder, Z. Shao, *iScience* **2020**, *23*, 100943.
- [90] B. W. Olbasa, F. W. Fenta, S.-F. Chiu, M.-C. Tsai, C.-J. Huang, B. A. Jote, T. T. Beyene, Y.-F. Liao, C.-H. Wang, W.-N. Su, H. Dai, B. J. Hwang, *ACS Appl. Energy Mater.* **2020**, *3*, 4499.
- [91] N. Palaniyandy, M. A. Kebede, K. Raju, K. I. Ozoemena, L. Le Roux, M. K. Mathe, R. Jayaprakasam, *Mater. Chem. Phys.* **2019**, *230*, 258.
- [92] S. H. Kim, S. M. Oh, *J. Power Sources* **1998**, *72*, 150.
- [93] Y. Fu, Q. Wei, G. Zhang, X. Wang, J. Zhang, Y. Hu, D. Wang, L. Zuin, T. Zhou, Y. Wu, S. Sun, *Adv. Energy Mater.* **2018**, *8*, 1801445.
- [94] C. Bischoff, O. Fitz, C. Schiller, H. Gentischer, D. Biro, H.-M. Henning, *Batteries* **2018**, *4*, 44.
- [95] J. Huang, Z. Wang, M. Hou, X. Dong, Y. Liu, Y. Wang, Y. Xia, *Nat. Commun.* **2018**, *9*, 2906.
- [96] D. L. Parkhurst, C. Appelo, *Techniques and Methods*, US Geological Survey, Reston, VA **2013**.
- [97] J. D. Allison, D. S. Brown, K. J. Novo-Gradac, *MINTEQA2/PRODEFA2, A Geographical Assessment Model for Environmental Systems: Version 3.0 User's Manual*, Environmental Research Laboratory, Office of Research and Development, U.S. Environmental Protection Agency, Athens, GA.
- [98] L. Wang, J. Zheng, *Mater. Today Adv.* **2020**, *7*, 100078.
- [99] J. Kielland, *J. Am. Chem. Soc.* **1937**, *59*, 1675.
- [100] E. Riche, A. Carrie, N. Andin, S. Mabic, *Am. Lab.* **2006**, *38*, 22.
- [101] H. N. Po, N. M. Senozan, *J. Chem. Educ.* **2001**, *78*, 1499.